Risks of Occupational Vibration Exposures

VIBRISKS

FP5 Project No. QLK4-2002-02650
January 2003 to December 2006

FIOSH

Annex 18 to Final Technical Report

Title: Whole-body vibration experimental work and biodynamic modelling

Authors: B. Hinz, H. Seidel, R. Blüthner, G. Menzel, J. Hofmann, L. Gericke, M. Schust, in cooperation with H. Kaiser and Ch. Mischke

Organisation: Federal Institute for Occupational Safety and Health, Germany

European Commission

Quality of Life and Management of Living Resources Programme
Key Action 4 - Environment and Health

10th January 2007

SUMMARY

Laboratory experiments with 21 male subjects were performed in order to examine human biodynamics during exposure to single-axis and multi-axis translational random whole-body vibration with different magnitudes. Effects of the factors vibration magnitude and number of axes were analysed. The results are presented as average apparent mass curves and transmissibilities with the associated coherencies. An existing anatomy-based numerical finite element model was extended to predict the load on the spine from combinations of static and dynamic compressive and shear forces arising from body posture and whole-body vibration. The model was validated by comparisons with experimental biodynamic data of FIOSH and partners. Based on representative postures and anthropometric data of European drivers obtained by partners, the basic model was modified in order to reflect typical postures and scaled to altogether 10 classes of body mass and body height, subdivided into two groups with a different body mass index. The model was applied to representative time histories measured in WP5. Model calculations were performed for different exposure conditions provided by partners, considering different postures and personal characteristics. The resulting forces acting on 6 different levels in 3 directions of the lumbar spine illustrate the significance of posture and personal characteristics for the prediction of spinal stress.

CONTENTS

Whole-Body Vibration - Experimental Work

1 Laboratory experiments

Two experimental studies involving 21 subjects were performed. For both studies the exposures were generated by the control system of the hexapod simulator modified for human experiments. The requirements of ISO 13090-1 were considered. For safety reasons a hip belt was used in all experiments.

To characterize the human biodynamics, the ways in which the vibration exposure is transmitted to and through the body were studied. Human biodynamics was quantified by the apparent masses at the seat- and feet-interface and the seat-to-head transmissibilities.

1.1 First experimental study

1.1.1 Exposure Conditions and Subjects

In the first study 13 subjects were exposed to single-axis vibration in X-, Y-, and Z-axis at three vibration magnitudes, dual-axis vibration in X- and Y-axis as well as three-axis vibration in X-, Y-, and Z-axis simultaneously at two vibration magnitudes. The excitation axes are marked by capitals, but measuring directions by lower-case letters (e.g. ax X means acceleration measured in x-direction during the excitation in X-axis). The subjects were exposed to random whole body vibration (nearly flat spectrum from 0.25 to 30 Hz for 60 s) with unweighted root mean square values (rms) of E1=0.26 ms^{-2}, E2=0.83 ms^{-2}, and E3=1.57 ms^{-2}. The twofold presentation of the vibration magnitudes and directions was balanced across the subjects.

The 13 male subjects had body masses between 61.3 and 103.6 kg (mean value (MV) 79.3 kg), and body heights between 173.5 and 197.0 cm (MV 184 cm). A total of 26 anthropometric parameters in the standing and 12 parameters in the sitting posture were measured. The subjects sat on the force plate, which was integrated in a rigid seat, with their ischial tuberosities approximately 20 to 30 cm from the front edge of the force plate and with the hands on a rigid support (cf. Figure 1, left). They were asked to adopt a comfortable, upright posture with normal muscle tension for the duration of each test. The feet were supported on a plate, 48.5 cm below the top surface of the force plate, with lower legs nearly vertical. The distance between the seat plate and feet plate was constant for all subjects.

1.1.2 Data acquisition

A force plate (Kistler 9396 AB) capable of measuring forces in three directions simultaneously was mounted as seat surface in order to measure forces in the fore-and-aft (x) direction, lateral (y) direction and vertical (z) direction. The force plate (60x40x20 cm) consisted of four tri-axial quartz piezoelectric transducers of the same sensitivity located at the four corners of the plate.

Signals from the force plate were amplified using an eight-channel amplifier (Kistler 9865 B). The feet were support by a second force plate (Kistler 9281 B12, SN 124804, 60x40x20 cm) together with an electronic unit (Kistler 9807).

The time series of the measured forces were corrected by subtracting the product of the mass of the plate resting on the force sensors and the acceleration measured at the seat plate for all conditions tested. This method was verified by measurements with rigid masses on the plates.

Accelerations in three translational directions (x, y, and z) were measured at the force plates using three capacitance accelerometers (ENDEVCO 7290A-10) mounted on special blocks for them (ENDEVCO 7990 block). The blocks were fixed on the right side of each of the Kistler force plates. The data acquisition was performed by a WaveBook (WBK16, Iotech).

A motion analysis system (Qualisys) was used to register the movements of body points (spinal process of C7, acromion process, elbow joint, wrist, pelvic, iliac crest, hip joint, knee joint, and ankle).

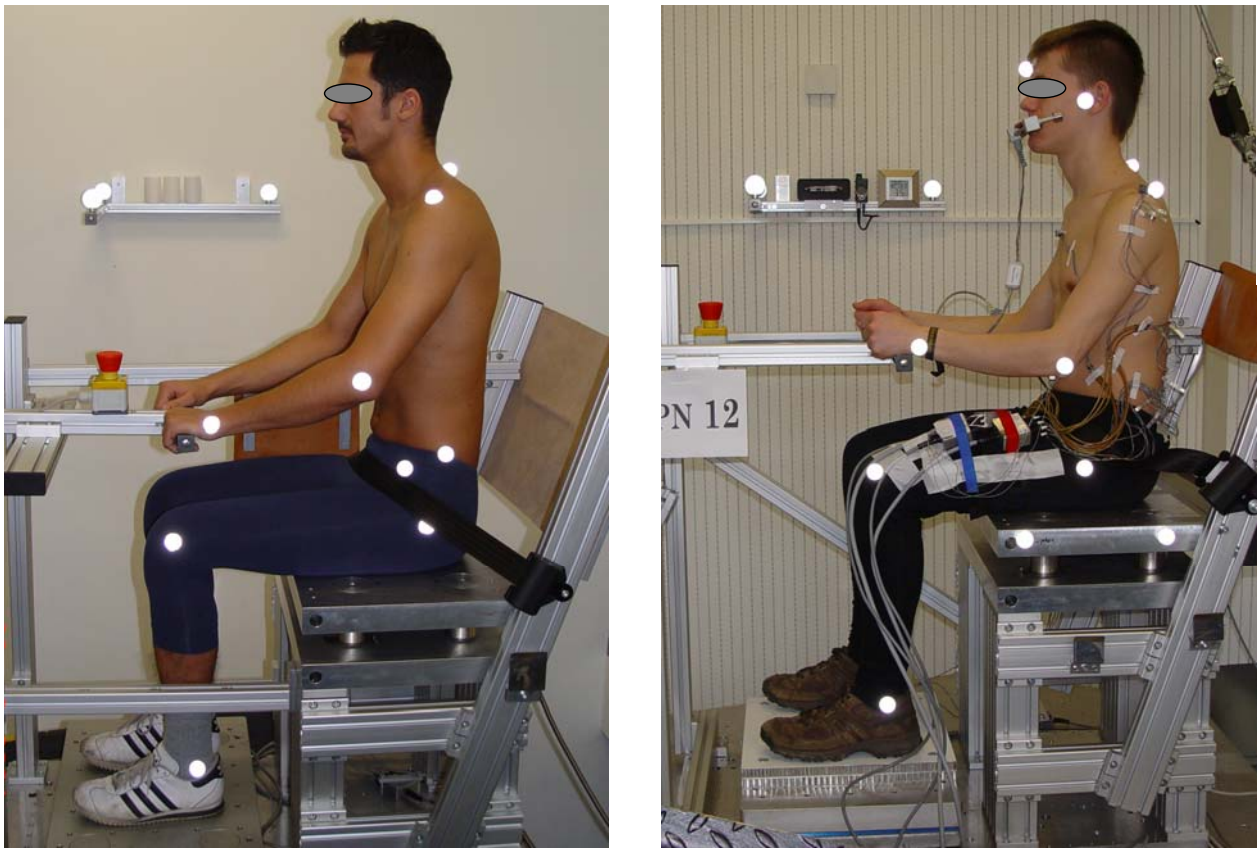

Figure 1 Subjects sitting on a rigid seat with an integrated force plate during the first experiment (left) and during the second experiment (right).

1.1.3 Data processing

The forces in the three translational directions were related to the input accelerations in the same direction and location.

The apparent mass (AM) is defined as the complex ratio of force amplitude (F) and acceleration amplitude (a) in the same direction (x, y, z) as a function of frequency (f). The apparent mass was calculated by dividing the cross spectral density function between the force (F) and the acceleration (a) by the power spectral density (P) of the seat acceleration using a MatLab routine.

$$AMx(f)=\frac{Fx(f)}{ax(f)} \qquad AMy(f)=\frac{Fy(f)}{ay(f)} \qquad AMz(f)=\frac{Fz(f)}{az(f)} \tag{1}$$

The associated coherence was calculated as

$$\gamma^2(Fx, ax)=\frac{|Fx\,ax(f)|^2}{Fx(f)\,ax(f)} \quad \gamma^2(Fy, ay)=\frac{|Fy\,ay(f)|^2}{Fy(f)\,ay(f)} \quad \gamma^2(Fz, az)=\frac{|Fz\,az(f)|^2}{Fz(f)\,az(f)} \tag{2}$$

The mean values of the moduli of the individual apparent masses were calculated by the usual averaging method. The calculations were performed for the apparent mass at the seat interface (AMS) and at the feet interface (AMF).

1.1.4 Results

1.1.4.1 AMS

The mean curves of the modulus determined by usual averaging show a clear dependence on the vibration magnitude for the single axis vibration (Figure 2, top).

The different amounts of shifts towards the lower frequencies with increasing vibration magnitudes are proportional to the differences of the levels of exposure intensities. The values of the coherency functions were in the range between 0.6 and 0.99 with the lower values at the higher frequencies (Figure 3, top).

The mean peak moduli tend to increase slightly across the intensities and directions. The main peak frequencies decreased with the increasing vibration magnitude.

The results during the dual- and three axis excitations showed that the apparent mass functions in the three measuring directions shifted to lower frequencies when the number of excitation axes increased from one to two or three (Figure 2, Hinz et. al, 2006). This phenomenon could have been caused by an increase of the vibration magnitude of the vector sum. The coherencies were in the same order as during the single axis excitation (Figure 3, middle and bottom).

1.1.4.2 AMF

The apparent masses at the feet showed comparable results with those of Nawayseh and

Griffin (2003) during the single Z-axis excitation and with those of Nawayseh and Griffin (2005) single X-axis excitation. The mean values of the apparent masses occurred at lower frequencies (Figure 4, top) for all conditions tested. The peak magnitudes decrease with the increasing vibration except during the single axis exposure in z-direction. During the dual- and three axis excitation similar changes were observed as for the AMS (Figure 4, middle and bottom).

The coherencies of AMF (Figure 5) reach lower values at lower frequencies as the coherencies of AMS. But in the range of the maxima of AMF the coherencies were found to be between 0.9 and 1.0.

Table 1. Minimum, maximum, mean values (N=26) and standard deviations (SD) for the frequencies (f) at which the maximum (max.) normalized (norm.) moduli of the apparent mass function (|AMS|) occurred in x-, y-, and z-direction during single-axis (X, Y, Z), dual-axis (XY), and three-axis (XYZ) excitations with the vibration magnitudes E1, E2, and E3.

	Minimum	Maximum	Mean	SD
Exposure 1 (E1)				
f (max. |AMS|) X x	2.38	4.00	2.94	0.42
f (max. |AMS|) XY x	2.00	4.50	2.94	0.57
f (max. |AMS|) XYZ x	2.00	4.00	2.82	0.46
f (max. |AMS|) Y y	1.13	2.75	2.04	0.31
f (max. |AMS|) XY y	1.63	2.75	2.11	0.29
f (max. |AMS|) XYZ y	1.75	2.75	2.19	0.29
f (max. |AMS|) Z z	3.38	6.63	5.14	0.96
f (max. |AMS|) XYZ z	3.13	6.25	4.71	0.89
Exposure 2 (E2)				
f (max. |AMS|) X x	1.75	3.00	2.45	0.28
f (max. |AMS|) XY x	1.13	3.00	2.29	0.36
f (max. |AMS|) XYZ x	1.25	4.00	2.40	0.44
f (max. |AMS|) Y y	1.13	2.38	1.62	0.32
f (max. |AMS|) XY y	1.13	2.38	1.66	0.38
f (max. |AMS|) XYZ y	1.13	2.25	1.61	0.29
f (max. |AMS|) Z z	3.5	5.88	4.69	0.77
f (max. |AMS|) XYZ z	3.38	5.63	4.31	0.85
Exposure 3 (E3)				
f (max. |AMS|) X x	1.63	2.50	2.18	0.19
f (max. |AMS|) Y y	1.13	1.75	1.37	0.19
f (max. |AMS|) Z z	3.25	5.63	4.41	0.69

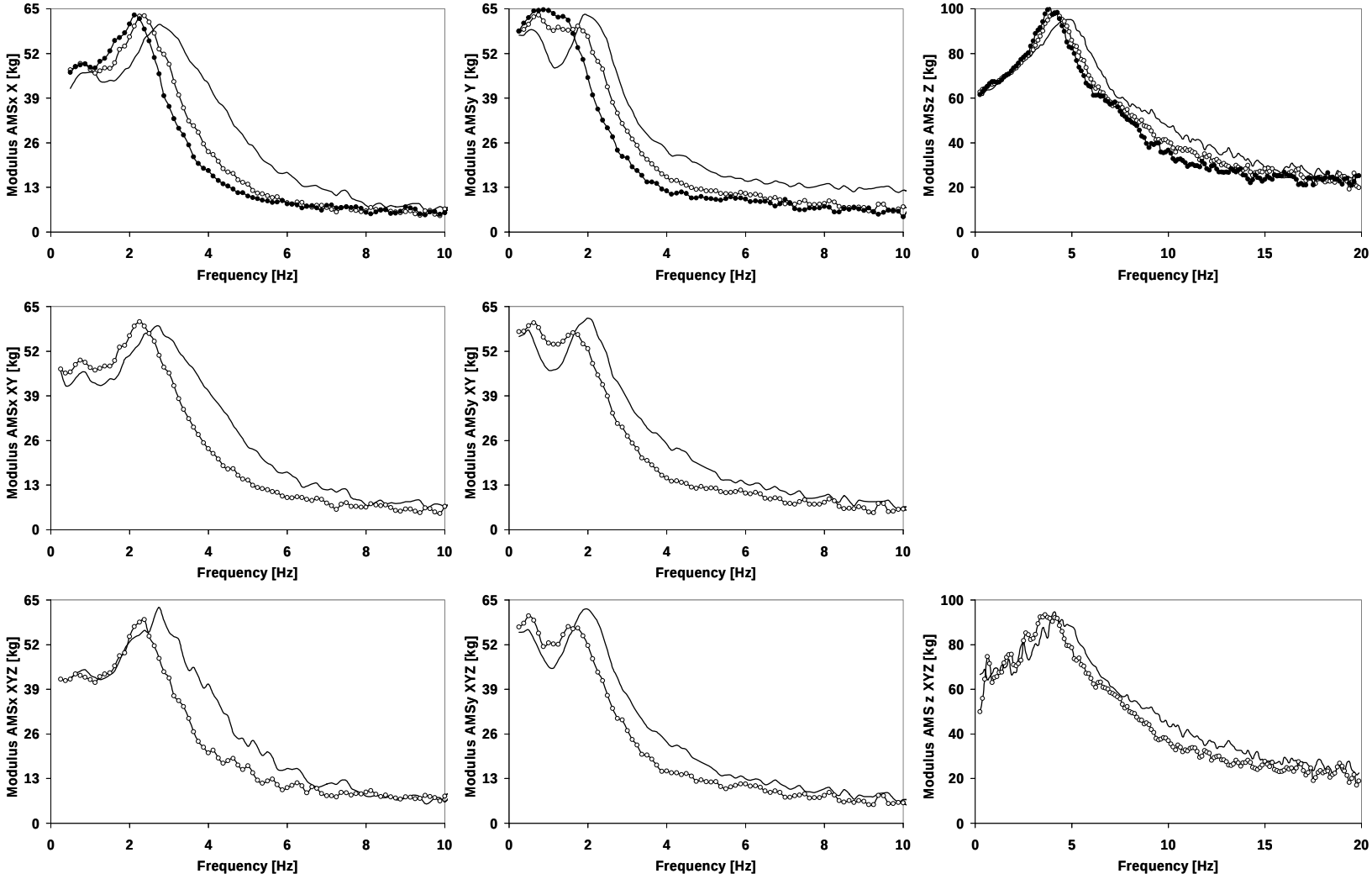

Figure 2. Mean values (MV) of the apparent masses in x- (left), y- (middle), and z-direction (right) at the seat interface (AMS) during the single-axis excitation (X, Y, Z - top), dual-axis excitation (XY - middle), three-axis excitation (XYZ - bottom). E1 (▬▬), E2 (○), E3 (●).

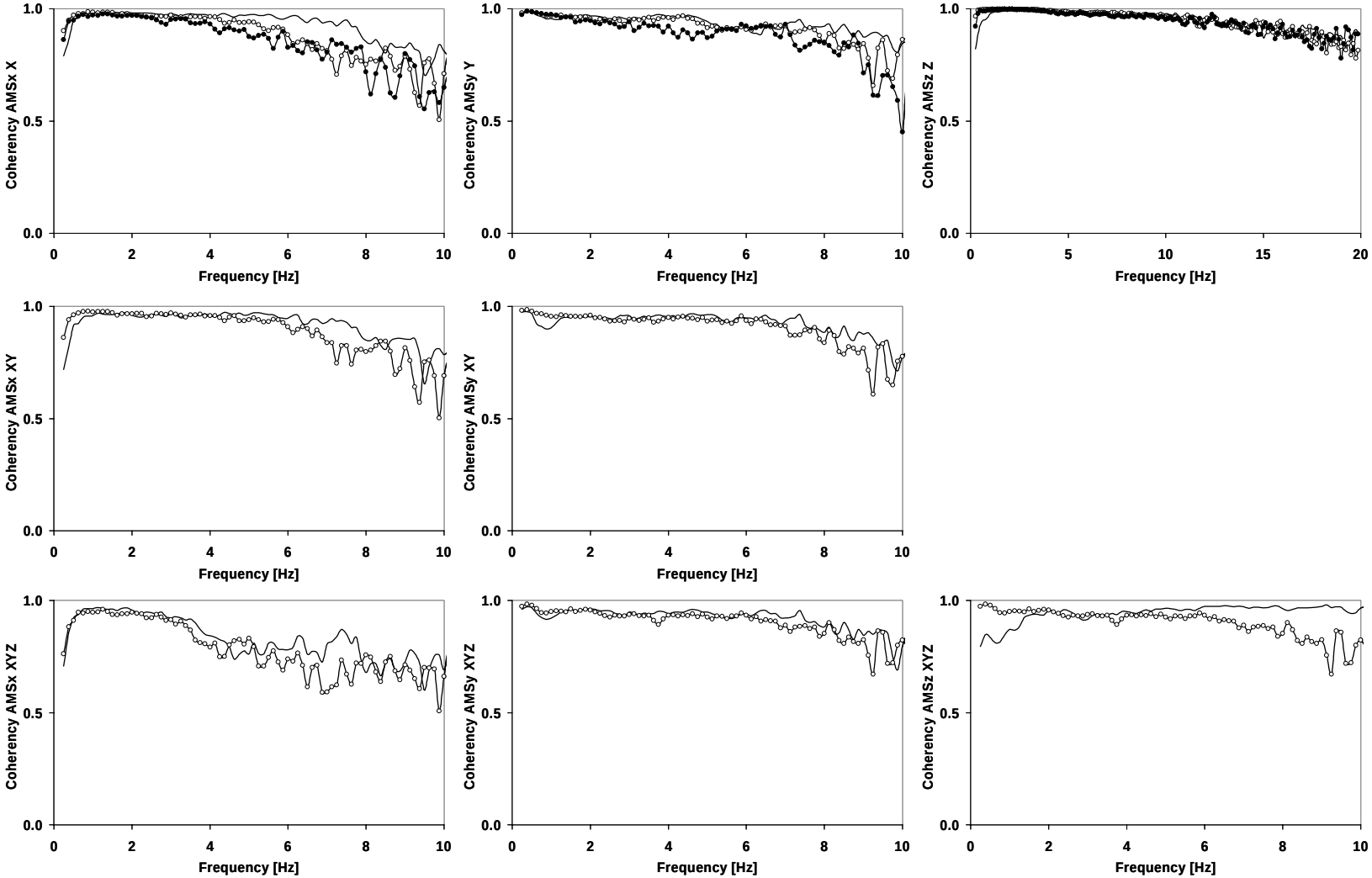

Figure 3. MV of coherencies associated with the apparent masses in x- (left), y- (middle), and z-direction (right) at the seat interface (AMS) during the single-axis excitation (X, Y, Z - top), dual-axis excitation (XY - middle), three-axis excitation (XYZ - bottom). E1 (——), E2 (○), E3 (●).

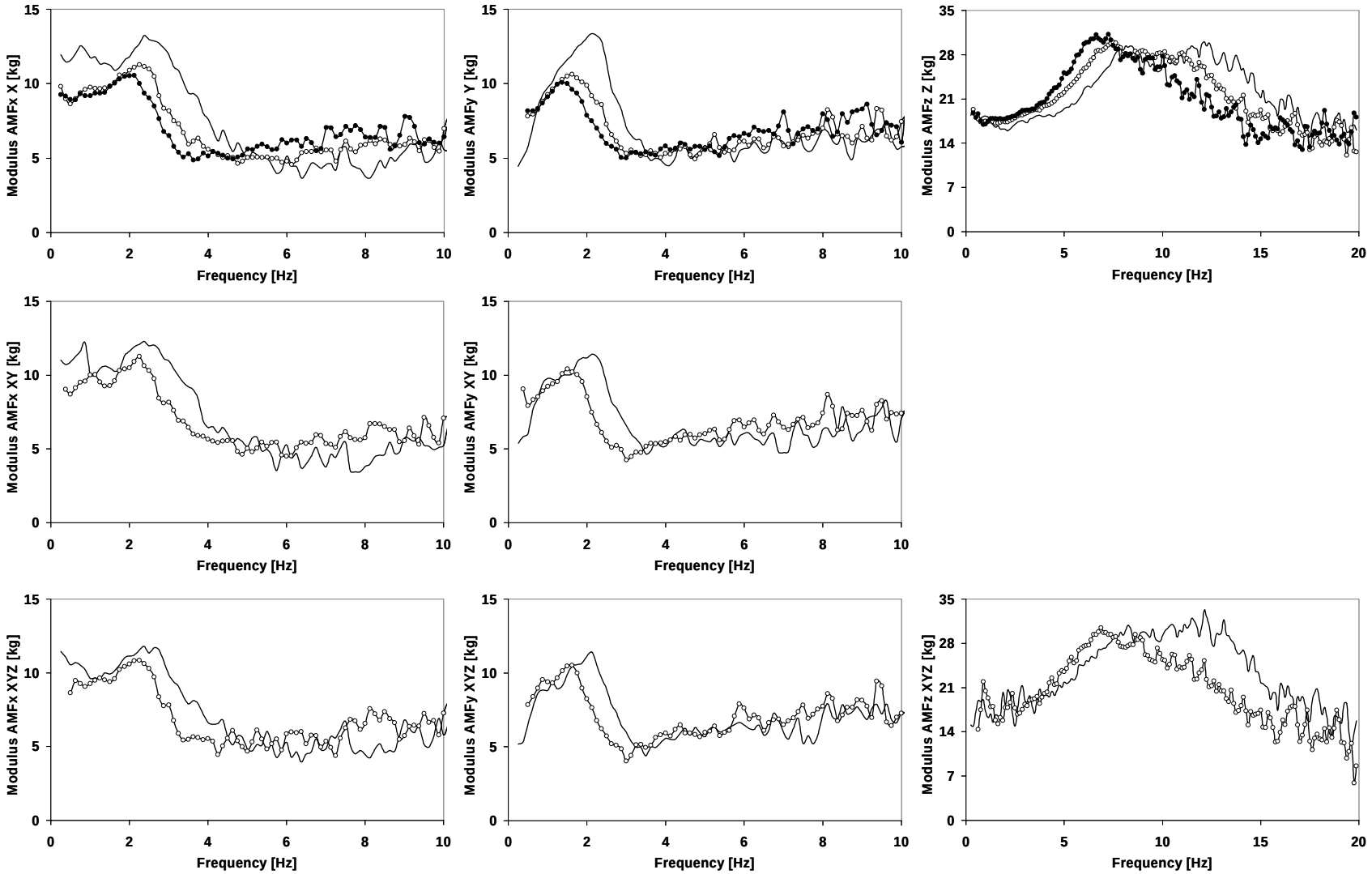

Figure 4. Mean values (MV) of the apparent masses in x- (left), y- (middle), and z-direction (right) at the feet interface (AMF) during the single-axis excitation (X, Y, Z - top), dual-axis excitation (XY - middle), three-axis excitation (XYZ - bottom). E1 (▬▬), E2 (○), E3 (●).

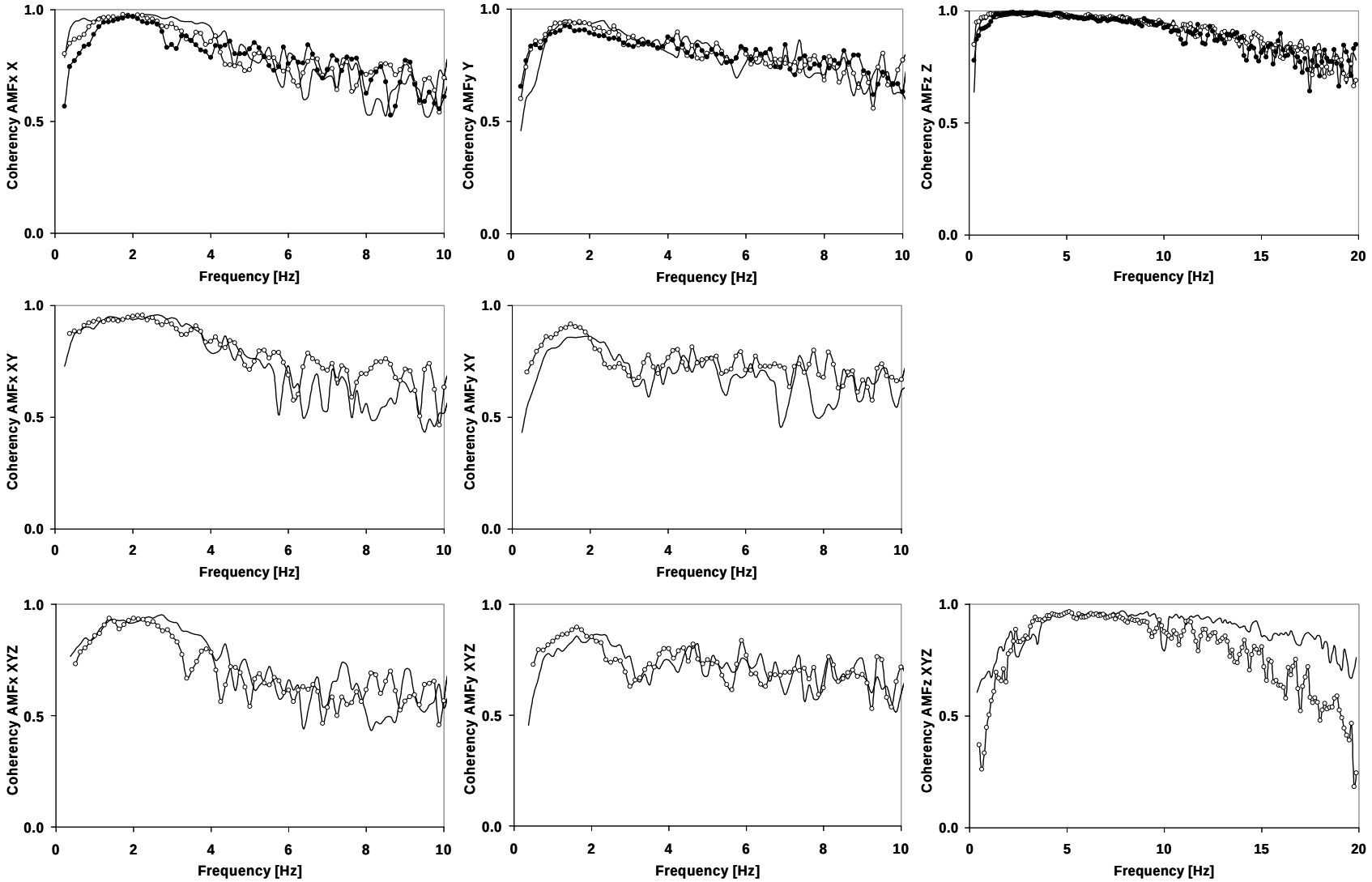

Figure 5. MV of coherencies associated with the apparent masses in x- (left), y- (middle), and z-direction (right) at the feet interface (AMf) during the single-axis excitation (X, Y, Z - top), dual-axis excitation (XY - middle), three-axis excitation (XYZ - bottom). E1 (——), E2 (○), E3 (●).

1.2 Second experimental study

1.2.1 Exposure Conditions and Subjects

In the second study 8 subjects were exposed at three vibration magnitudes to single-axis vibration in X, Y, and Z axis and to three-axis vibration in X, Y, and Z axis simultaneously. The excitation axes are marked by capitals, but measuring directions by lower-case letters (e.g. ax X means acceleration measured in x-direction during the excitation in X axis). The subjects were exposed to random whole body vibration (nearly flat spectrum from 0.25 to 20 Hz for 65 s) with unweighted rms values of I1=0.45 ms^{-2}, I2=0.90 ms^{-2}, and I3=1.80 ms^{-2}. The twofold presentation of the vibration magnitudes and directions was balanced across the subjects.

The 8 male subjects had body masses between 64 and 105.9 kg (mean value (MV) 85 kg), and body heights between 173.5 and 197.0 cm (MV 185 cm). A total of 26 anthropometric parameters in the standing and 12 parameters in the sitting posture were measured. The subjects sat on the force plate, which was integrated in a rigid seat, with their ischial tuberosities approximately 20 to 30 cm from the front edge of the force plate and with the hands on a support. They were asked to adopt a comfortable, upright posture with normal muscle tension for the duration of each test. The feet were supported by a second force plate. The seat height was individually adapted by additional plates (aluminium sandwich construction "ALUCORE Aluminiumverbundplatten, mejo Metall Joslen GmbH&Co.KG") mounted on the feet plate to get a constant body angle between thighs and lower legs of about 90 degrees (cf. Figure 1, right).

1.2.2 Data acquisition

A force plate (Kistler 9396 AB) capable of measuring forces in three directions simultaneously was mounted as seat surface in order to measure forces in the fore-and-aft (x) direction, lateral (y) direction and vertical (z) direction. The force plate (60x40x20 cm) consisted of four tri-axial quartz piezoelectric transducers of the same sensitivity located at the four corners of the plate. Signals from the force plate were amplified using an eight-channel amplifier (Kistler 9865 B). The feet were support by a second force plate (Kistler 9281 B12, SN 124804, 60x40x20 cm) together with an electronic unit (Kistler 9807).

The time series of the measured forces were corrected by subtracting the product of the mass of the plate resting on the force sensors and the acceleration measured at the seat plate for all conditions tested. The masses of additional plates were considered, too. This method was verified by measurements with rigid masses on the plate.

Accelerations in three translational directions (x, y, and z) were measured at each force plate

using six capacitance accelerometers (ENDEVCO 7290A-10) mounted on two special blocks for them (ENDEVCO 7990 block). Each block was fixed on the right side of each of the Kistler force plates.

Translational accelerometers mounted on a bite bar (material: titan) to measure head motion were full bridge piezo-resistive (strain gauge) type accelerometers (2 EGAXT3-M-10 and 1 EGAXT-10, Entran). The bite bar was held by the teeth via an individually produced bite plate (Impression Compound, SPOFA-Dental, Praha). The head accelerations were measured in three directions (cf. Figure 6).

The data acquisition was performed by a WaveBook (WBK16, Iotech).

A motion analysis system (Qualisys) was used to register the movements of body points (spinal process of C7, acromion process, elbow joint, wrist, pelvic, iliac crest, hip joint, knee joint, and ankle).

1.2.3 Data processing

The forces in the three translational directions were related to the input accelerations in the same direction and location.

The apparent mass (AM) is defined as the complex ratio of force amplitude (F) and acceleration amplitude (a) in the same direction (x, y, z) as a function of frequency (f). The apparent mass was calculated by the cross spectral density method using a MatLab routine according to formula (1) and (2). The mean values of the moduli of the individual apparent masses were calculated by the usual averaging method. The calculations were performed for the apparent mass at the seat interface (AMS) and at the feet interface (AMF).

The translational head accelerations were measured by the three dimensional accelerometers. The accelerations of the centre of gravity of the bite bar were calculated using the six measured accelerations with the associated distances l_1, l_2, l_3 and the inverted transformation matrix considering the coordinates of the accelerometer (origin: centre of gravity, cf. Figure 6).

$$\begin{bmatrix} \ddot{z}_1 \\ \ddot{x}_2 \\ \ddot{y}_2 \\ \ddot{z}_2 \\ \ddot{x}_3 \\ \ddot{z}_3 \end{bmatrix} = \begin{bmatrix} 0 & 0 & 1 & -l_2 & l_1 & 0 \\ 1 & 0 & 0 & 0 & 0 & l_2 \\ 0 & 1 & 0 & 0 & 0 & 0 \\ 0 & 0 & 1 & -l_2 & 0 & 0 \\ 1 & 0 & 0 & 0 & 0 & -l_3 \\ 0 & 0 & 1 & l_3 & 0 & 0 \end{bmatrix} \begin{bmatrix} a_x \\ a_y \\ a_z \\ a_{\varphi x} \\ a_{\varphi y} \\ a_{\varphi z} \end{bmatrix} \tag{3}$$

The calculation using the inverted matrix delivered the translational (a) and rotational head accelerations (a_φ):

$$a_x = [l_3 * \ddot{x}_2 + \ddot{x}_3 * l_2]/(l_3 + l_2) \qquad a_{\varphi x} = (\ddot{z}_3 - \ddot{z}_2)/(l_3 + l_2) \tag{4}$$

$$a_y = \ddot{y}_2 \qquad a_{\varphi y} = (\ddot{z}_1 - \ddot{z}_2)/l_1 \tag{5}$$

$$a_z = [l_2 * \ddot{z}_3 + \ddot{z}_2 * l_3]/(l_3 + l_2) \qquad a_{\varphi z} = (\ddot{x}_2 - \ddot{x}_3)/(l_3 + l_2) \tag{6}$$

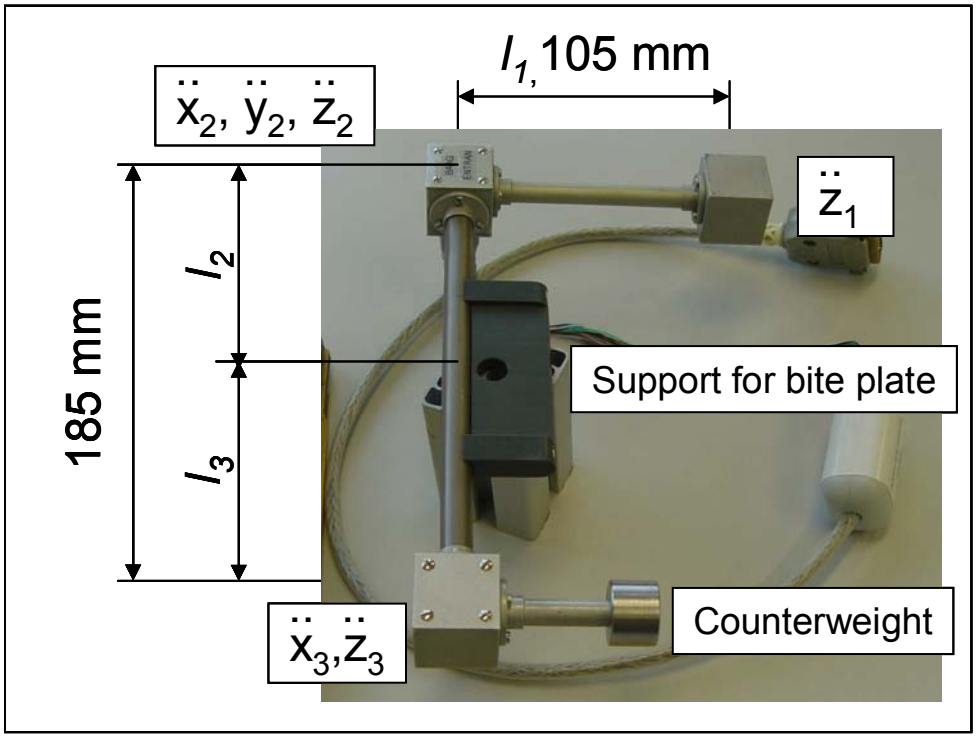

Figure 6. Photography of the bite bar with the main information about the locations of accelerometers, distances between them. The hole in support can prevent relative movements between the support and the bite plate especially if the mass of the bite plate is pressed into the hole.

All possible seat-to-head transfer functions were calculated by dividing the cross spectral density functions (CPSD) between the seat acceleration (a) and the head acceleration (ha) by the power spectral density (PSD) of the seat acceleration (7). The according coherencies were determined according to equation (8).

$$T(f) = \frac{CPSD(a, ha)}{PSD(a)} \qquad \gamma^2(f) = \frac{|(CPSD\ (a, ha)|^2}{P(a, a)\ P(ha, ha)} \tag{7, 8}$$

The mean values of the magnitudes of the individual seat-to-head transfer functions were

calculated by the usual averaging method.

1.2.4 Results

1.2.4.1 AMS

The mean values of the AMS during the single- and three axis excitations confirmed the results of the first experiment concerning the dependence of the moduli of AMS on the vibration magnitude as well as on the number of axes of the excitation (Figure 7). The peak values of AMS were higher than in the first experiment, possibly caused by the different vibration magnitudes exposed, the higher masses of the subjects and/or the changed posture of the legs (constant angle between thigh and lower leg).
Lower values than in the first experiment were registered for the coherencies especially for the excitation in X-axis above 3 Hz and for the excitation in Y-axis above 2 Hz. In the range of the maxima of AMS the values of coherencies were in the range between 0.9 and 1.0 (Figure 8).

1.2.4.2 AMF

The mean values of AMF showed in the horizontal direction slightly higher values and in z-direction slightly lower values than in the first experiment (Figure 9). The dependence of the frequencies at which the maximum of AMF occurred on the number of axes was more distinct than in the first experiment (cf. Figure 9, top and bottoms).
The coherencies were not lower than 0.8 in the whole frequency range (Figure 10) except in y-direction around 3 Hz (Figure 10 middle, top and bottom). These higher coherencies may result to a certain amount from the better contact of feet with the force plate caused by the constant knee angle.

1.2.4.3 Transmission of vibration to the head

1.2.4.3.1 Transmission of single-axis seat vibration to the head (X, Y, Z)

This section describes the transmission of single-axis seat vibration (ax, ay, az) to the translational and rotational head movements (hax, hay, haz; rothax, rothay, rothaz). During the excitation in *X-axis* the peak values of the mean head transmissibility *hax/ax* occurred around 1 Hz with magnitudes between 1.2 and 2.3 with the lower values at the higher vibration magnitudes (Figure 11, top, left). The values of the peak magnitudes of the transfer functions were slightly higher than those reported by Paddan and Griffin (1988b), whereas the peak frequencies coincided. The transmissibility *hay/ax* (Figure 11, top, middle) meets the results of Paddan and Griffin (1988b), but the peak magnitudes were in the order of 0.2 occurring around 2 Hz. The results of the associated coherency indicate a relatively small reliability in this

transmission (Figure 12, top, middle). The transmissibility *haz/ax* showed a clear dependence on the vibration magnitude (Figure 11, top, right).
Excitations in X-axis were described (Paddan and Griffin, 1988b) to result in head motions within the mid-sagittal plane (x-z plane). The transmissibilities *rothay/ax* (Figure 15, top, middle) showed mean peak magnitudes between 5 and 12 rad/m with the lower values at the higher vibration magnitudes supported by mean coherencies of about 0.8 in the range of peaks around 2 Hz (Figure 16, top, middle). The maxima of the mean magnitudes of the transmissibilities *rothax/ax* (Figure 15, top, left) and *rothaz/ax* (Figure 15 top, right) occurred in the same frequency range, but the magnitudes were lower than 1.8. The coherencies with mean values lower than 0.5 indicate a relatively low reliability (Figure 16 top, left and right).

During the excitation in *Y-axis* the peak values of the mean transmissibility *hay/ay* (Figure 11, middle, middle) occurred around 1 Hz with magnitudes between 1.5 and 2.4. The transmissibilities *hax/ay* (Figure 11, middle, left) and *haz/ay* (Figure 11, middle, right) delivered no characteristic patterns and magnitudes of the transfer functions below 0.4 and 0.2, respectively. The low values of the mean coherencies (Figure 12, middle, left and right) – below 0.5 – hint to a missing relation between the input at the seat and the output at the head. The results of Paddan and Griffin (1988b) showed also very low values, but the coherencies were not discussed.
Excitations in Y-direction resulted in head movements around the X-axis and - to a clearly lower extent - around the z-axis. The mean values of the transmissibility *rothax/ay* (Figure 15, middle, left) reached maximum values between 4 and 10 rad/m in the frequency range between 1 and 2 Hz. The mean coherencies supported the results by values around 0.8 in the range of the peak (Figure 16, middle, left). The transmissibility *rothaz/ay* (Figure 15, middle, right) reached mean maximum magnitudes below 5 rad/m, but these values were relatively constant between 2 and 4 Hz. In this frequency range the associated mean coherencies were in the order of 0.5 to 0.6 (Figure 16, middle, right). The relation *rothay/ay* delivered very low values (Figure 15, middle, middle) accompanied by mean coherencies around 0.2 (Figure 16, middle, middle) Paddan and Griffin (1988b) came to similar results, but with slightly lower magnitudes.

During the excitation in *Z-axis* the mean peak values of the transmission *haz/az* occurred in the range between 1.8 and 2.4 at frequencies around 6 Hz (Figure 11, bottom, right). The dependence of the vibration magnitude confirmed earlier results (Paddan and Griffin, 1988a, Hinz et al. 2001). A second smaller peak was detected between 10 and 15 Hz. The mean coherencies were nearly 1 during all three vibration magnitudes in the whole frequency range tested (Figure 12, bottom, right). The transmissibilities *hax/az* and *hay/az* (Figure 11 bottom, left and middle) have the peak frequencies around 5 Hz, too. But the maximum magnitudes

were clearly lower with mean values below 0.6. The mean values of the coherencies were a sign of certain reliability (Figure 12, bottom, left and middle).
During the excitations in Z-axis head motions occurred in the x- and z-direction combined with rotations mainly around the Y-axis (Paddan and Griffin, 1988a). This finding can be confirmed. For the transmissibilities rothay/az maxima of mean magnitudes in the range between 7 and 11 rad/m were found (Figure 15, bottom, middle). The values showed a clear dependence on the intensity. The mean peak frequencies were registered between 5 and 7 Hz. The mean coherences amounted to about 0.7 to 0.9 for frequencies higher than 4 Hz. For the mean values of the transmissibilities rothax/az and rothaz/az were registered clearly lower maximum magnitudes with values between 1 and 2.8 rad/m. Peaks occurred around 5 Hz (except of rothax/az during the lowest vibration magnitude). The mean values of the coherencies in the order of 0.5 to 0.8 speak for a certain reliability of the results.

1.2.4.3.2 Transmission of three-axis seat vibration to the head (XYZ)

This section describes the transmission of three-axis seat vibration (ax, ay, az) to the translational and rotational head movements (hax, hay, haz; rothax, rothay, rotahz). In general the curves of seat-to-head transmissibilities during the three-axis vibration have a jagged course compared with the seat-to-head transmissibilities during single-axis vibration. For the majority of conditions tested sharp points in the curves at the very low frequencies were associated with relatively low coherencies.
Compared with the single-axis inputs, the dependence of the transmissibilities on the vibration magnitude remained nearly unchanged, but the increased number of axes seems to have an additional effect due to an increase of the vibration total value.
In comparison wit the coherencies at the single-axis excitations the mean values of the coherency functions were lower during the three-axis excitations in the whole frequency range tested or in the range of higher frequencies only.
To the author's knowledge a comparison between the seat-to-head transmissibility during one-and-three axis excitation has not been reported so far.
During the excitation in *XYZ-axis* the peak values of the mean head transmissibility in *x-direction* *hax/ax* in the range between 1.2 and 2.4 occurred around 1 Hz (Figure 13, top, left). In the range of the peak values the mean coherencies amounted to about 0.7 (Figure 14, top, left). The mean transmissibilities *haz/ax* showed the same pattern as during single-axis excitation, but the curves were more rugged (Figure 13, top, right). The coherencies reached in the peak range maximum values around 0.5 (Figure 14, top, right). For the mean transmissibilities *hay/ax* the values were lower than 1 (Figure 13, top, middle) and the associated coherencies indicated an insufficient reliability (Figure 14, top, middle).
During the excitation in *XYZ*-axis the transmissibilities *rothay/ax* (Figure 17, top, middle)

showed mean peak magnitudes between 4 and 10 rad/m with the lower values at the higher vibration magnitudes supported by mean coherencies of about 0.8 in the range of peaks around 2 Hz (Figure 18, top, middle). The magnitudes during the three-axis vibration were lower than during single axis vibration. For the transmissibilities *rothax/ax* and *rothaz/ax* the dependence on the frequency had an unclear profil (Figure 17, top, left and right) and the mean values of coherencies were lower than 0.2 (Figure 18, top, left and right).

During the excitation in *XYZ-axis* the mean head transmissibility in *y-direction hay/ay* had no remarkable peaks, but increased continuously from 2 to 0 Hz (Figure 13, middle, middle). The coherencies reach acceptable values of about 0.8 in a very narrow frequency range between about 0.7 and 1.7 (Figure 14, middle, middle). The transmissibilities *hax/ay* and *haz/ay* reached relatively low values (Figure 13, middle, left and right) accompanied by coherencies around 0.1 (Figure 14, middle, left and right) – similarly to the relation during single axis excitation in Y-direction.

During the excitation in *XYZ*-axis the head transmissibilities *rothax/ay* and *rothaz/az* showed nearly the same pattern (Figure 17, middle, left and right) as during single axis vibration. The expected differences concerning the shift of curves to the lower frequencies seem to occur. Also the coherencies (Figure 18, middle, left and right) were nearly in the same range as during the single axis excitation at frequencies below 6 Hz.

During the excitation in *XYZ-axis* the main peak values of the mean head transmissibility *in z-direction haz/az* occurred between 5 and 6 Hz (Figure 13, bottom, right) with a lower magnitude than during single-axis vibration. The second peak remained nearly unchanged concerning the magnitude. Both peaks occurred at lower frequencies than during the single axis excitation during each vibration magnitude. The coherencies were in the expected range above 4 Hz (Figure 14, bottom, right). The transmissibilities *hax/az* show relatively low maximum values of nearly 0.6 rad/m (Figure 13, bottom, left) associated with mean coherencies in of about 0.7 to 0.8 in the frequency range of these peaks around 5 Hz (Figure 14, bottom,left). The coherencies were lower than 0.5 for the transmissibility *hay/az* (Figure 14, bottom, middle) and indicated a less reliability of these transmissibilities (Figure 13, bottom, middle).

During the excitation in *XYZ*-axis the head transmissibility *rothay/ax* demonstrated the peak values between 2 and 3 Hz, i.e. at lower frequencies than during single-axis vibration. Also the magnitudes were lower (Figure 17, top, middle). The coherencies remained nearly unchanged in the frequency range of the peaks (Figure 18, top, middle). The transmissibilities *rothax/ax* and *rothaz/ax* had high small narrow peak magnitudes (Figure 17, top, right and left), but the coherencies below 0.5 hint to a low reliability of the data (Figure 18, top, right and left). Compared with the single-axis excitation the shape of the transmissibilities *rothax/ay* and *rothaz/ay* during the three-axis excitation was nearly unchanged with slightly lower magnitudes

(Figure 17, middle, left and right). Also the coherencies were slighty lower (Figure 18, middle, left and right). The transmissibilities *rothay/y* seem not to be caused by the input vibration (Figure 17, middle, middle) due to the coherencies lower than 0.2 (Figure 18, middle, middle). The peak magnitudes of the transmissibilities *rothay/az* were lower than 9 rad/m and occurred around 5 Hz with a shift of the curves to lower frequencies with increasing vibration magnitudes (Figure 17, bottom, middle). A similar effect can be observed by a comparison with the same transfer functions during single-axis excitation (Figure 15, bottom, middle). The coherencies were in the range between 0.5 and 0.8 (Figure 18, bottom, middle). The transmissibilities *rothax/az* and *rothaz/az* showed numerous narrow peaks (Figure 17, bottom, left). The associated coherencies were no higher than 0.5 indicating a less reliability of these transmission values (Figure 18, bottom, left).

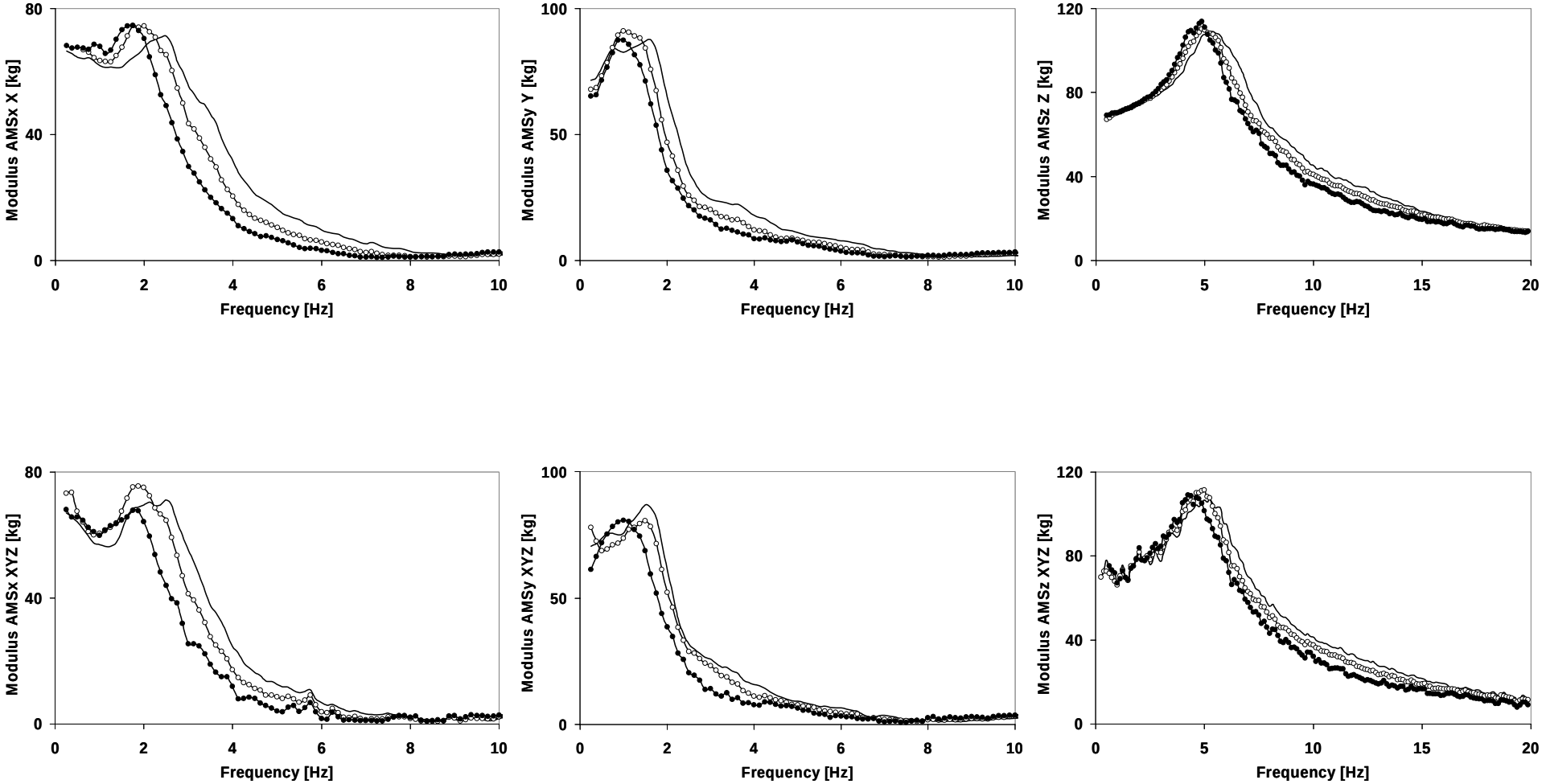

Figure 7. Mean values (MV) of the apparent masses in x- (left), y- (middle), and z-direction (right) at the seat interface (AMS) during single-axis excitation (X, Y, Z - top) and three-axis excitation (XYZ - bottom). I1 (——), I2 (○), I3 (●).

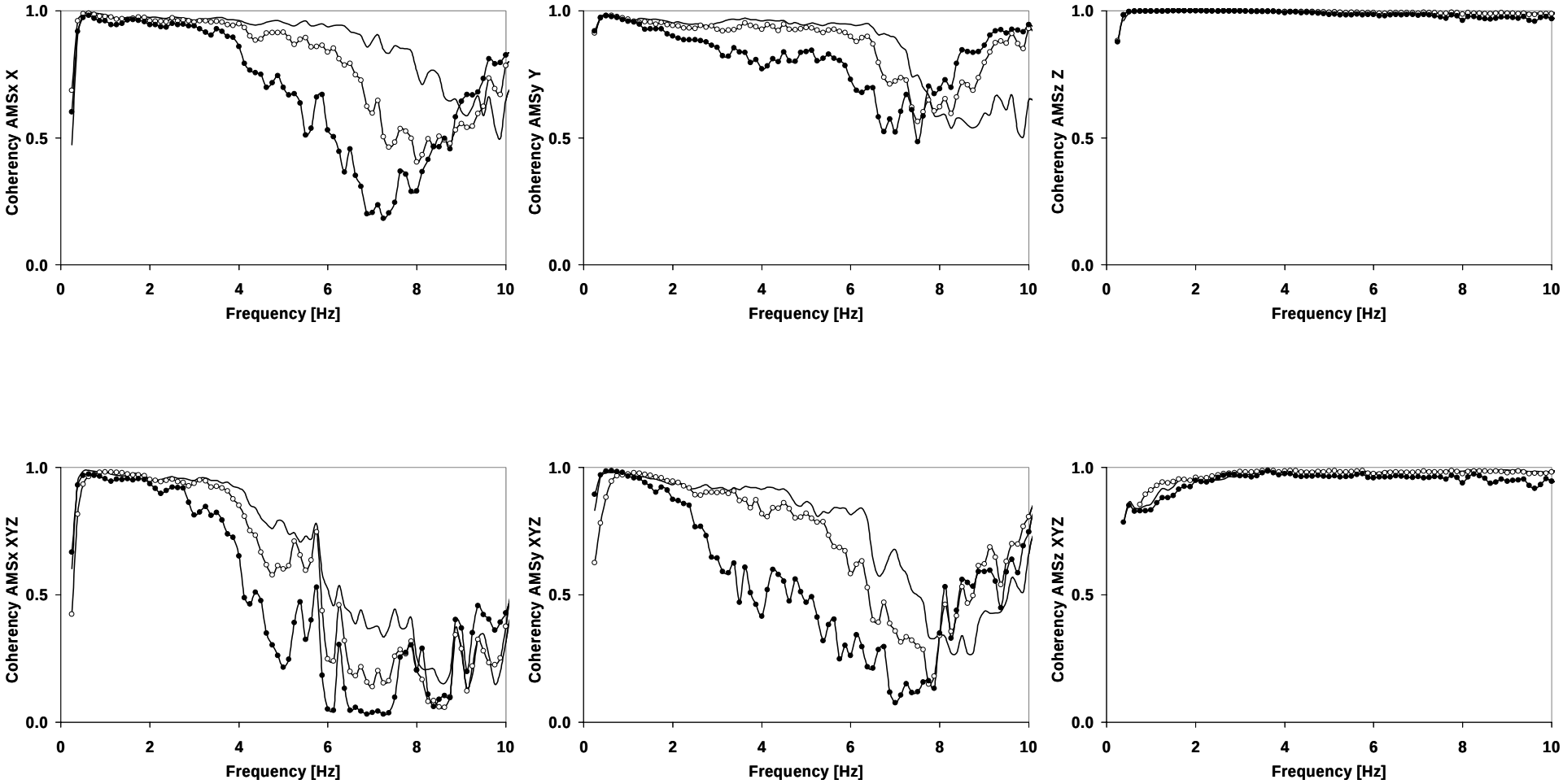

Figure 8. MV of coherencies associated with the apparent masses in x- (left), y- (middle), and z-direction (right) at the seat interface (AMS) during single-axis excitation (X, Y, Z - top) and three-axis excitation (XYZ – bottom. I1 (——), I2 (○), I3 (●).

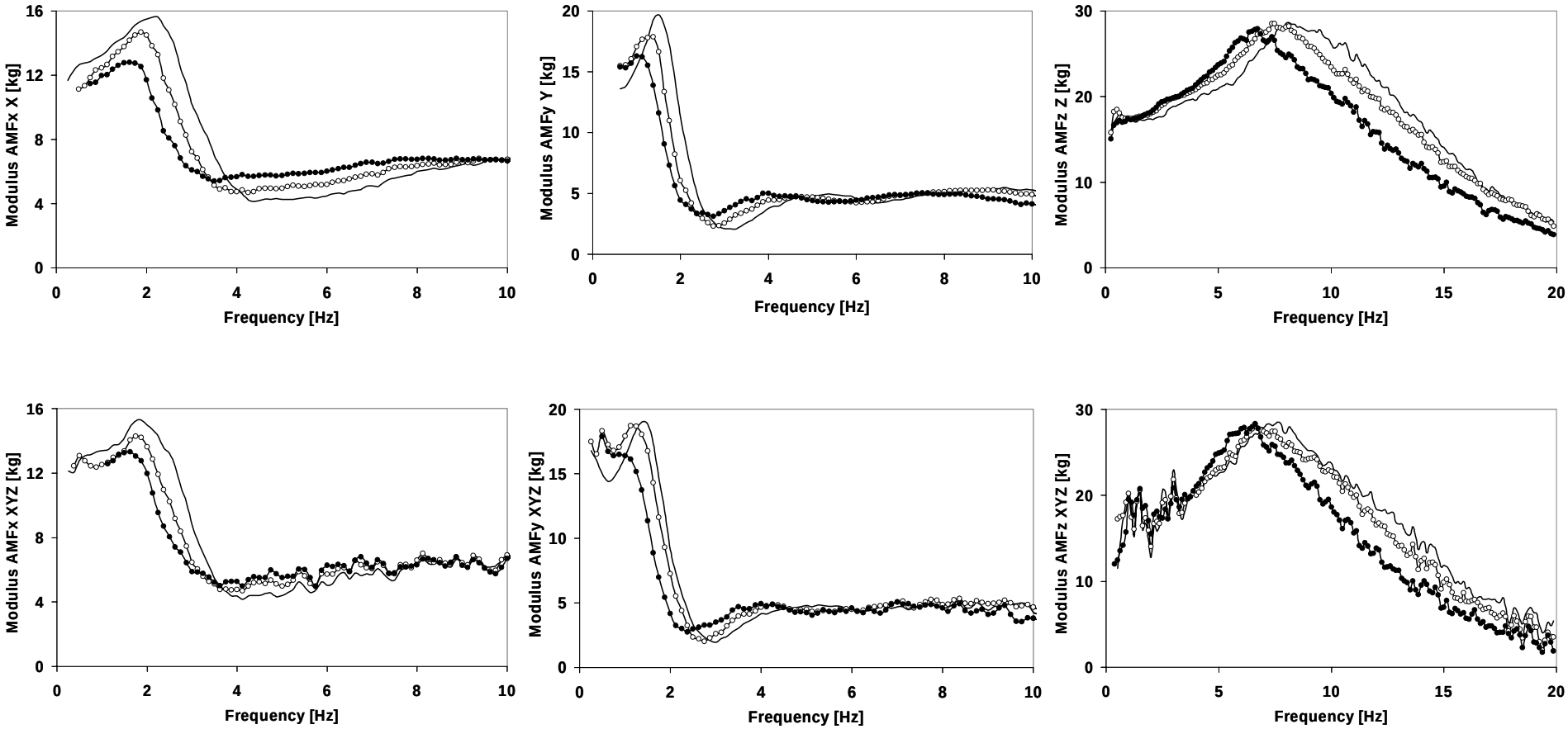

Figure 9. Mean values (MV) of the apparent masses in x- (left), y- (middle), and z-direction (right) at the feet interface (AMF) during single-axis excitation (X, Y, Z - top) and three-axis excitation (XYZ - bottom). I1 (——), I2 (○), I3 (●).

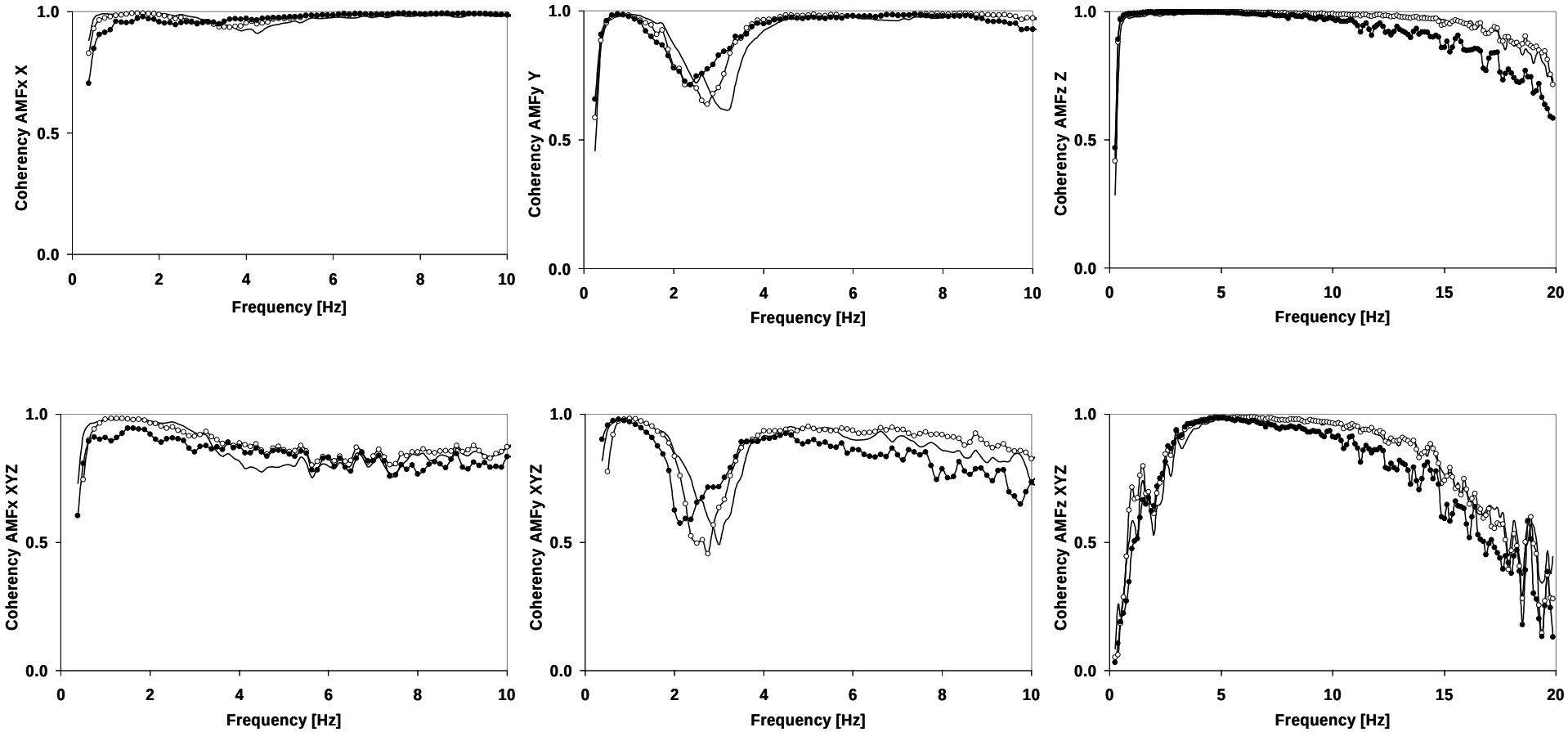

Figure 10. MV of coherencies associated with the apparent masses in x- (left), y- (middle), and z-direction (right) at the feet interface (AMF) during single-axis excitation (X, Y, Z - top) and three-axis excitation (XYZ - bottom). I1 (——), I2 (○), I3 (●).

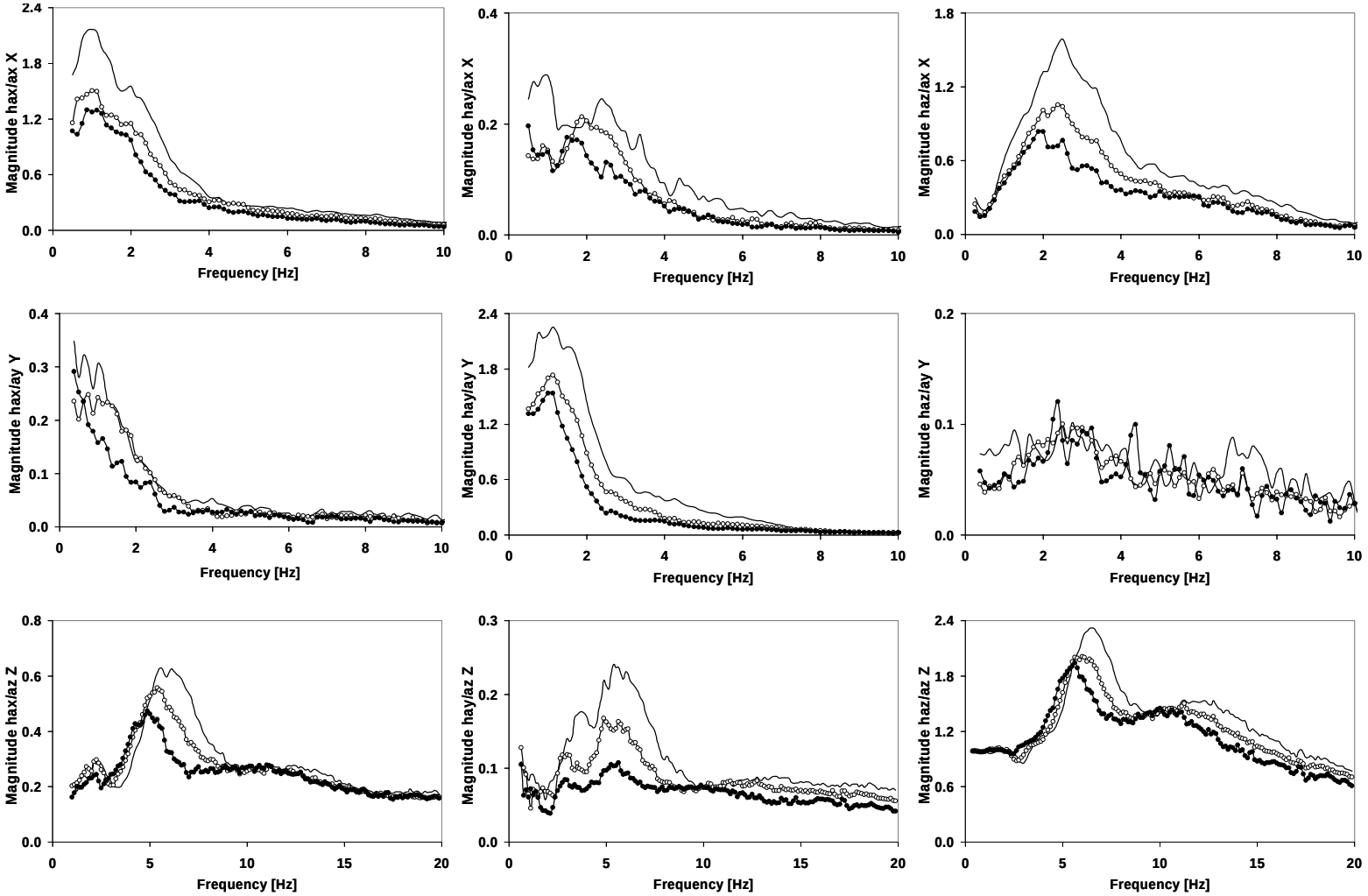

Figure 11. Mean values (MV) of the magnitudes of the seat-to-head transfer functions during single-axis vibration in X-axis (top), in Y-axis (middle) and in Z-axis (bottom). The seat accelerations were related to the head acceleration in x-direction (left), in y-direction (middle) and in z-direction (right). I1 (▬▬), I2 (○), I3 (●), a - acceleration at the seat. ha - acceleration of the head, rot hx - roll acceleration at the head, rot hy - pitch acceleration at the head, rot hz - yaw acceleration at the head.

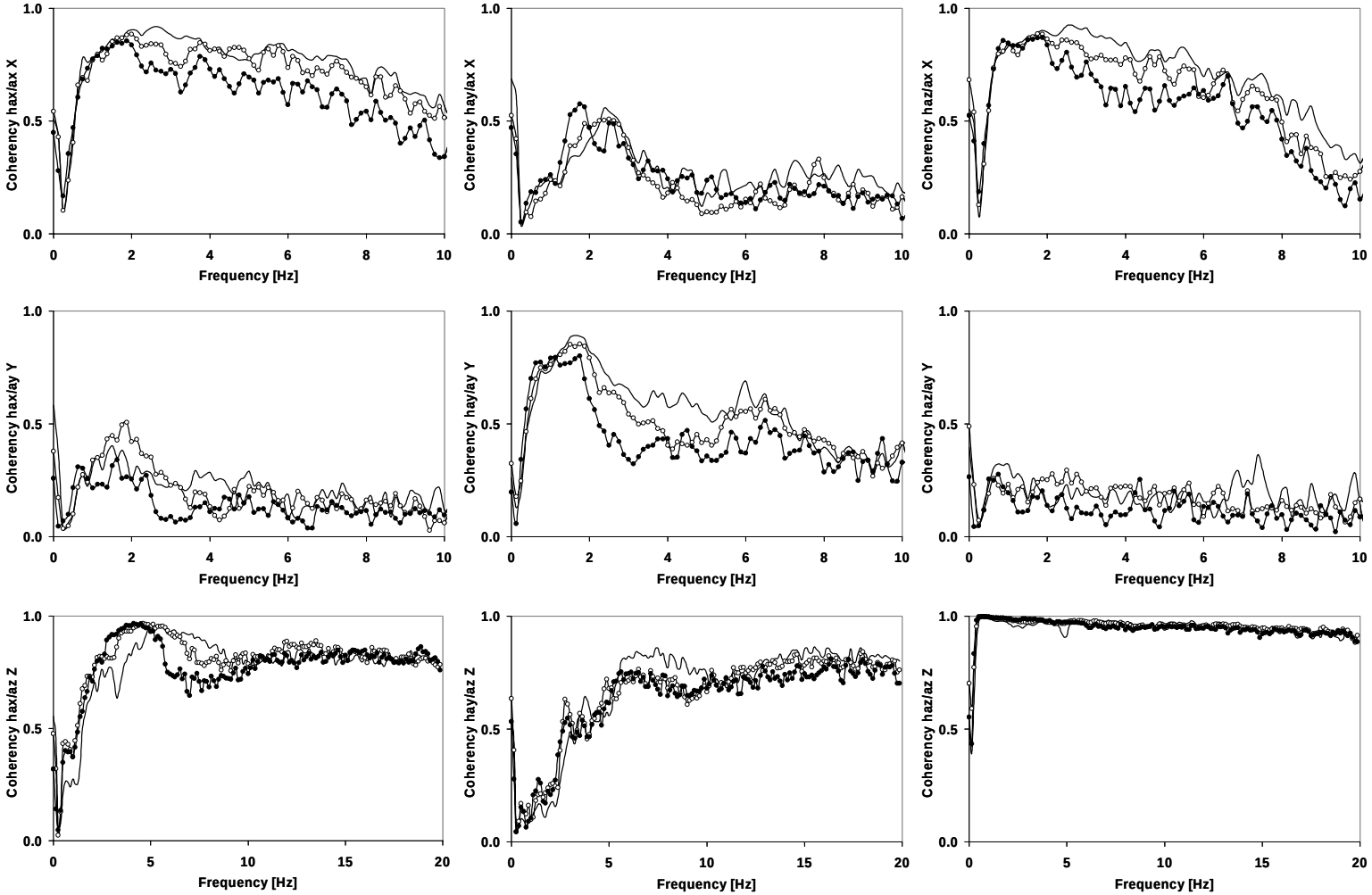

Figure 12: Mean values (MV) of the coherencies associated with the seat-to-head transfer functions during single-axis vibration in X-axis (top), in Y-axis (middle) and in Z-axis (bottom). The seat accelerations were related to the head acceleration in x-direction (left), in y-direction (middle) and in z-direction (right). I1 (▬▬), I2 (○), I3 (●).a - acceleration at the seat. ha - acceleration of the head, rot hx - roll acceleration at the head, rot hy - pitch acceleration at the head, rot hz - yaw acceleration at the head.

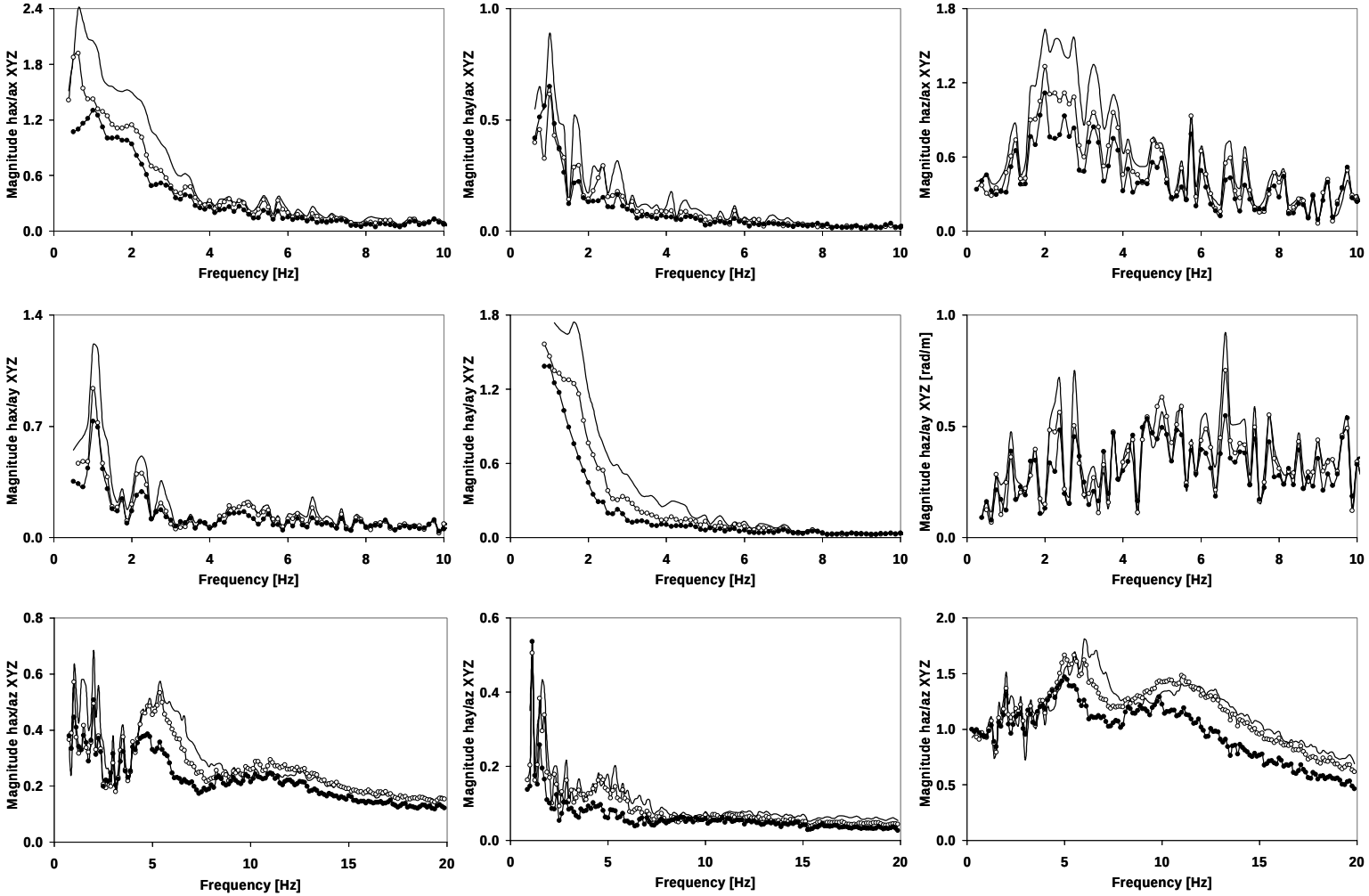

Figure 13. Mean values (MV) of the magnitudes of the seat-to-head transfer functions during three-axis vibration simultaneously in X-, Y-, and in Z-axis. The seat accelerations in x-direction (top), y-direction (middle) and z-direction were related to the head acceleration in x-direction (left), in y-direction (middle) and in z-direction (right). I1 (▬▬), I2 (○), I3 (●).a - acceleration at the seat. ha - acceleration of the head, rot hx - roll acceleration at the head, rot hy - pitch acceleration at the head, rot hz - yaw acceleration at the head.

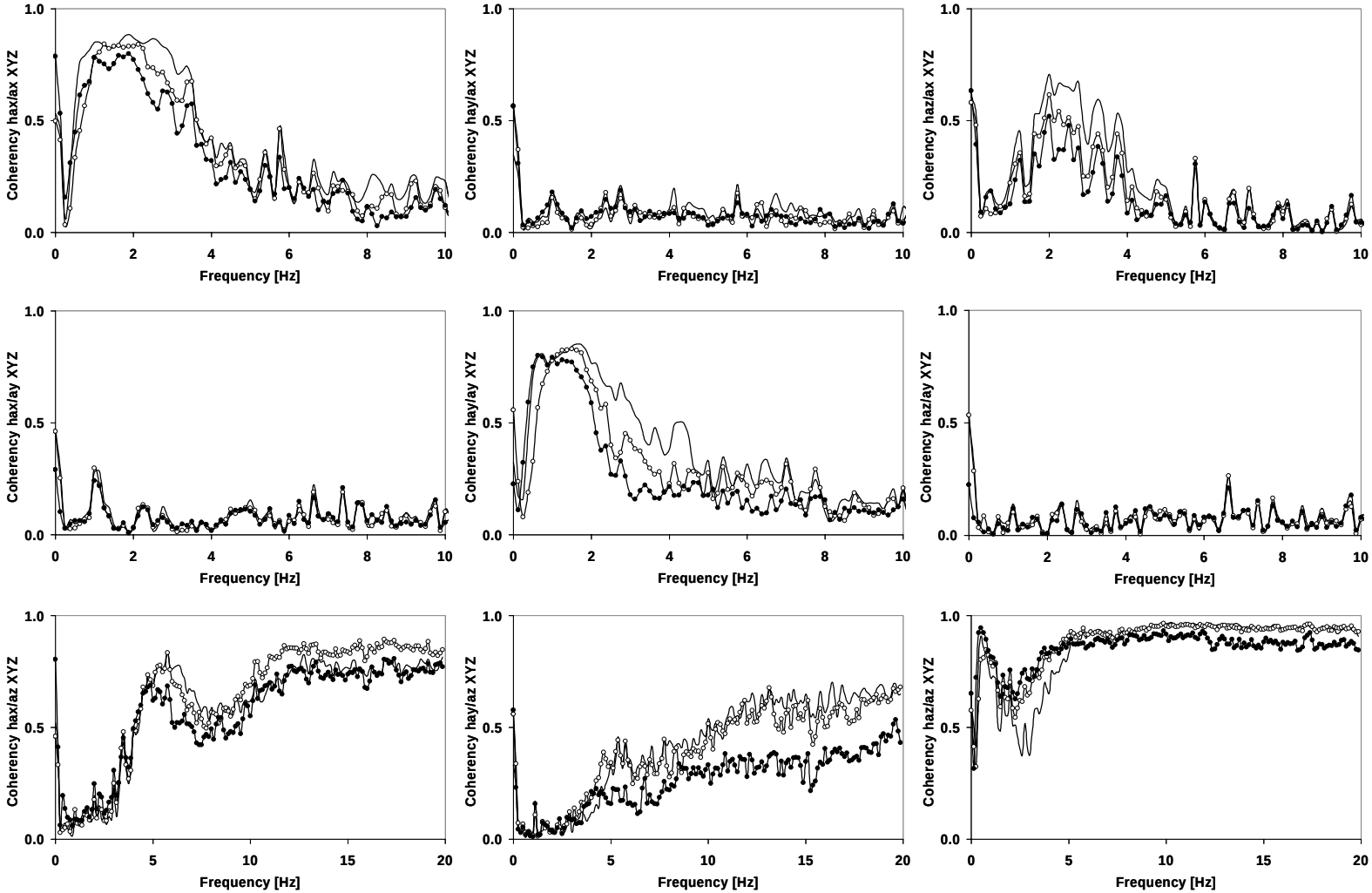

Figure 14. Mean values (MV) of the coherencies associated with the seat-to-head transfer functions during three-axis vibration simultaneously in X-, Y-, and in Z-axis. The seat accelerations in x-direction (top), y-direction (middle) and z-direction were related to the head acceleration in x-direction (left), in y-direction (middle) and in z-direction (right). I1 (——), I2 (○), I3 (●).a - acceleration at the seat. ha - acceleration of the head, rot hx - roll acceleration at the head, rot hy - pitch acceleration at the head, rot hz - yaw acceleration at the head.

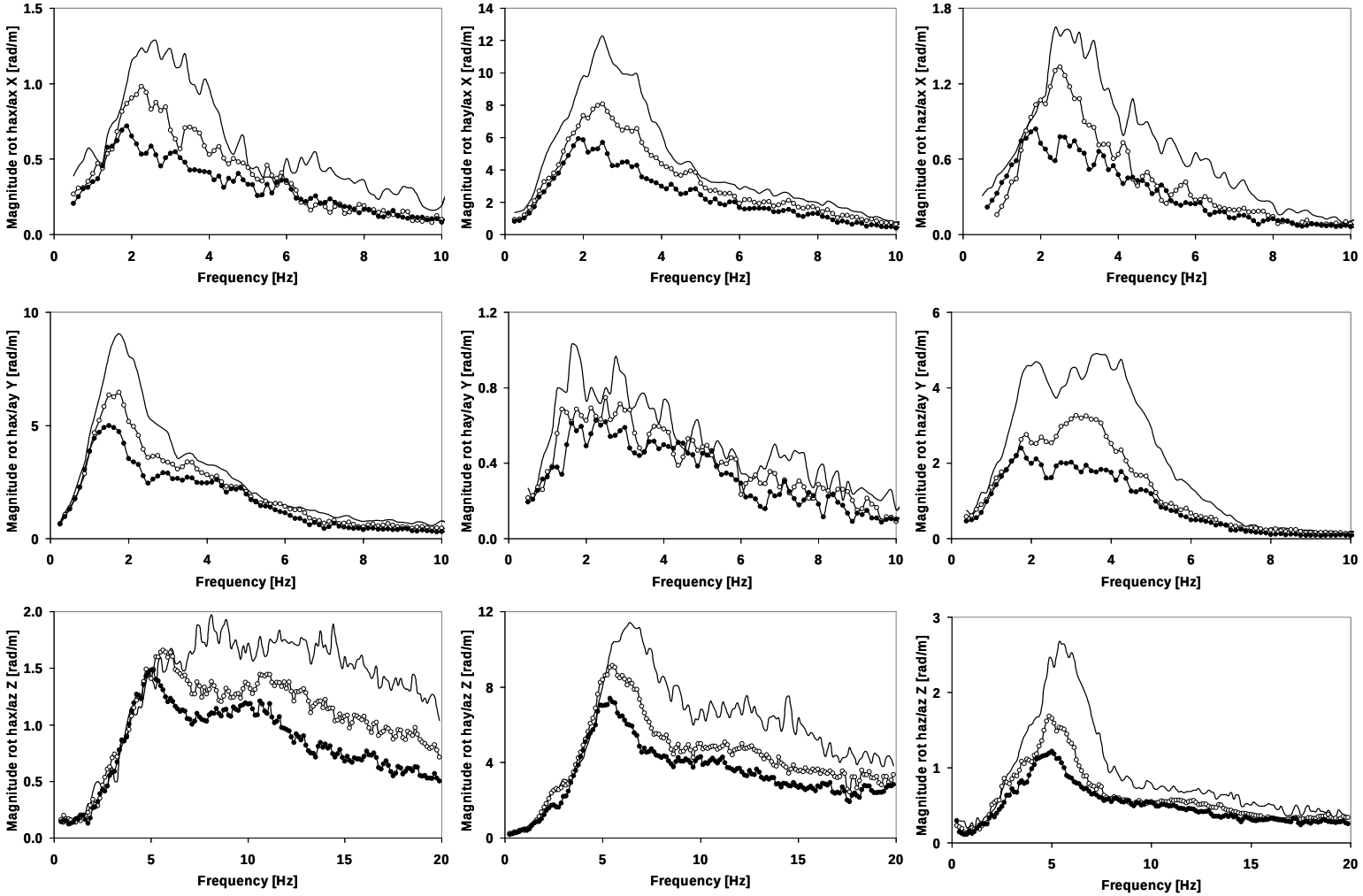

Figure 15. Mean values (MV) of the magnitudes of the seat-to-head transfer functions during single-axis vibration in X-axis (top), in Y-axis (middle) and in Z-axis (bottom). The translational seat accelerations were related to the rotational head accelerations around x-direction (left), around y-direction (middle) and around z-direction (right). I1 (▬▬), I2 (○), I3 (●).a - acceleration at the seat. ha - acceleration of the head, rot hx - roll acceleration at the head, rot hy - pitch acceleration at the head, rot hz - yaw acceleration at the head.

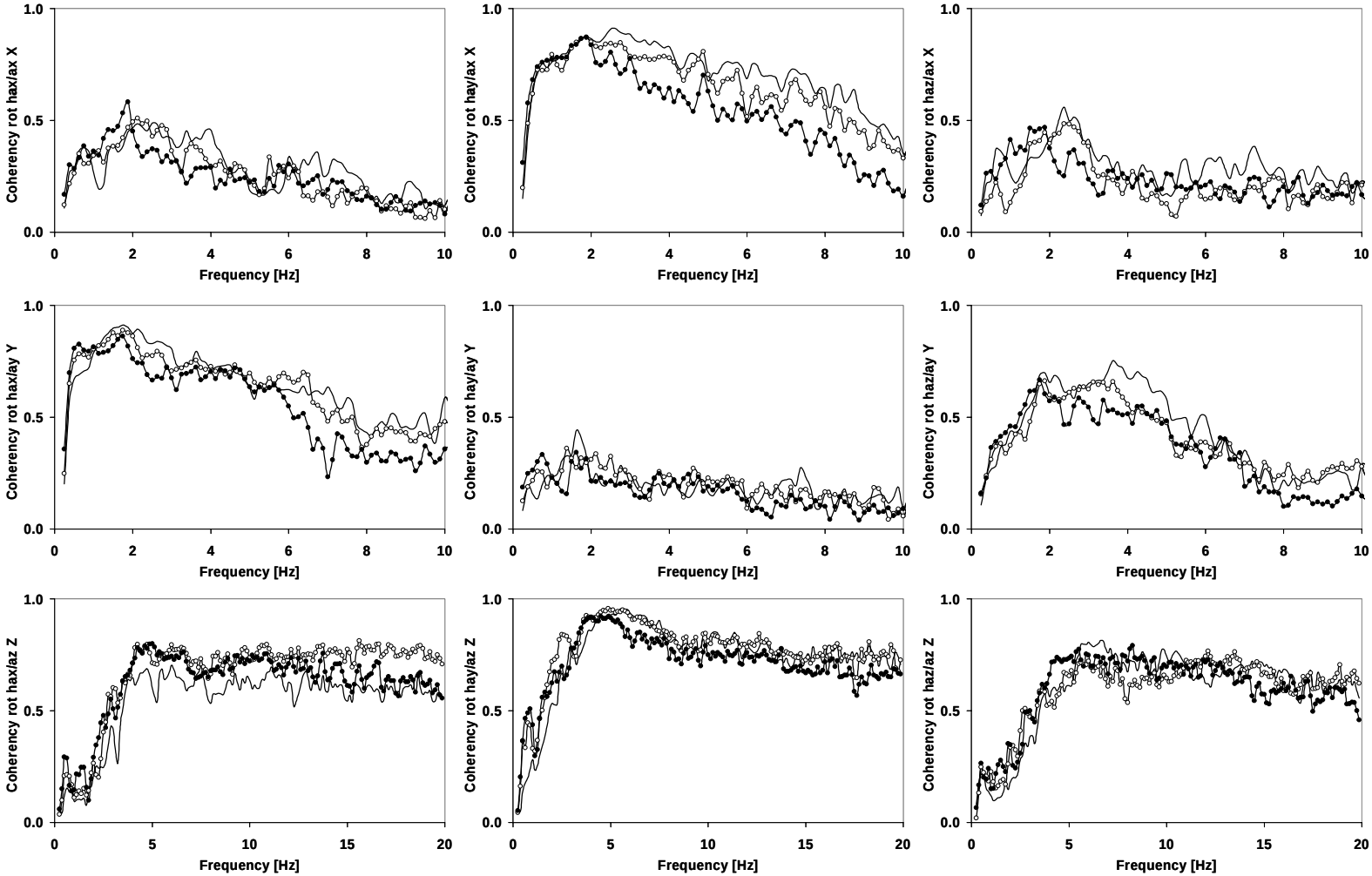

Figure 16. Mean values (MV) of the coherencies associated with the seat-to-head transfer functions during single-axis vibration in X-axis (top), in Y-axis (middle) and in Z-axis (bottom). The translational seat accelerations were related to the rotational head accelerations around x-direction (left), around y-direction (middle) and around z-direction (right). I1 (▬▬), I2 (○), I3 (●).a - acceleration at the seat. ha - acceleration of the head, rot hx - roll acceleration at the head, rot hy - pitch acceleration at the head, rot hz - yaw acceleration at the head.

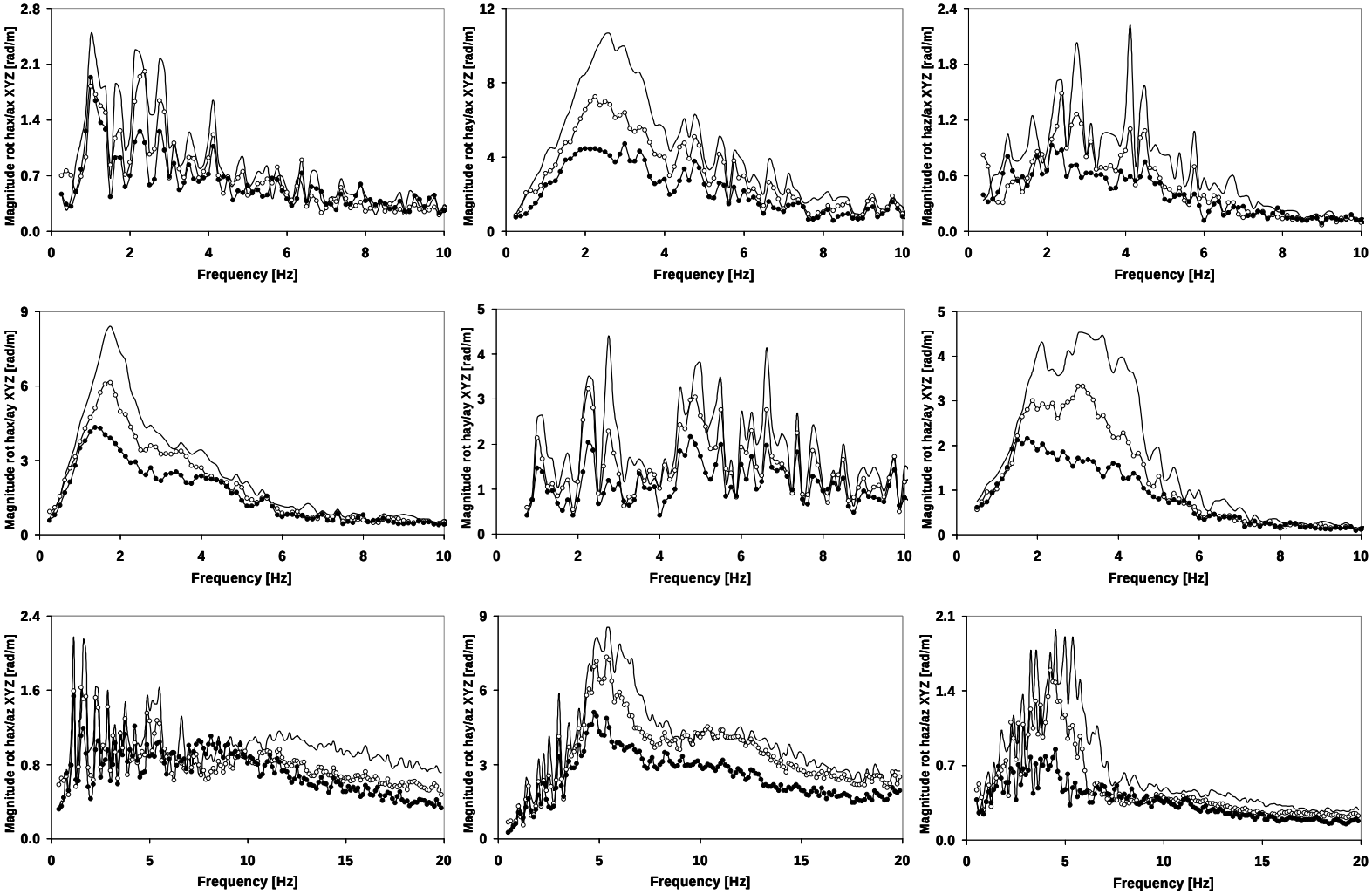

Figure 17. Mean values (MV) of the magnitudes of the seat-to-head transfer functions during three-axis vibration simultaneously in X-, Y-, and in Z-axis. The translational seat accelerations were related to the rotational head accelerations around x-direction (left), around y-direction (middle) and around z-direction (right). I1 (▬▬), I2 (○), I3 (●).a - acceleration at the seat. ha - acceleration of the head, rot hx - roll acceleration at the head, rot hy - pitch acceleration at the head, rot hz - yaw acceleration at the head.

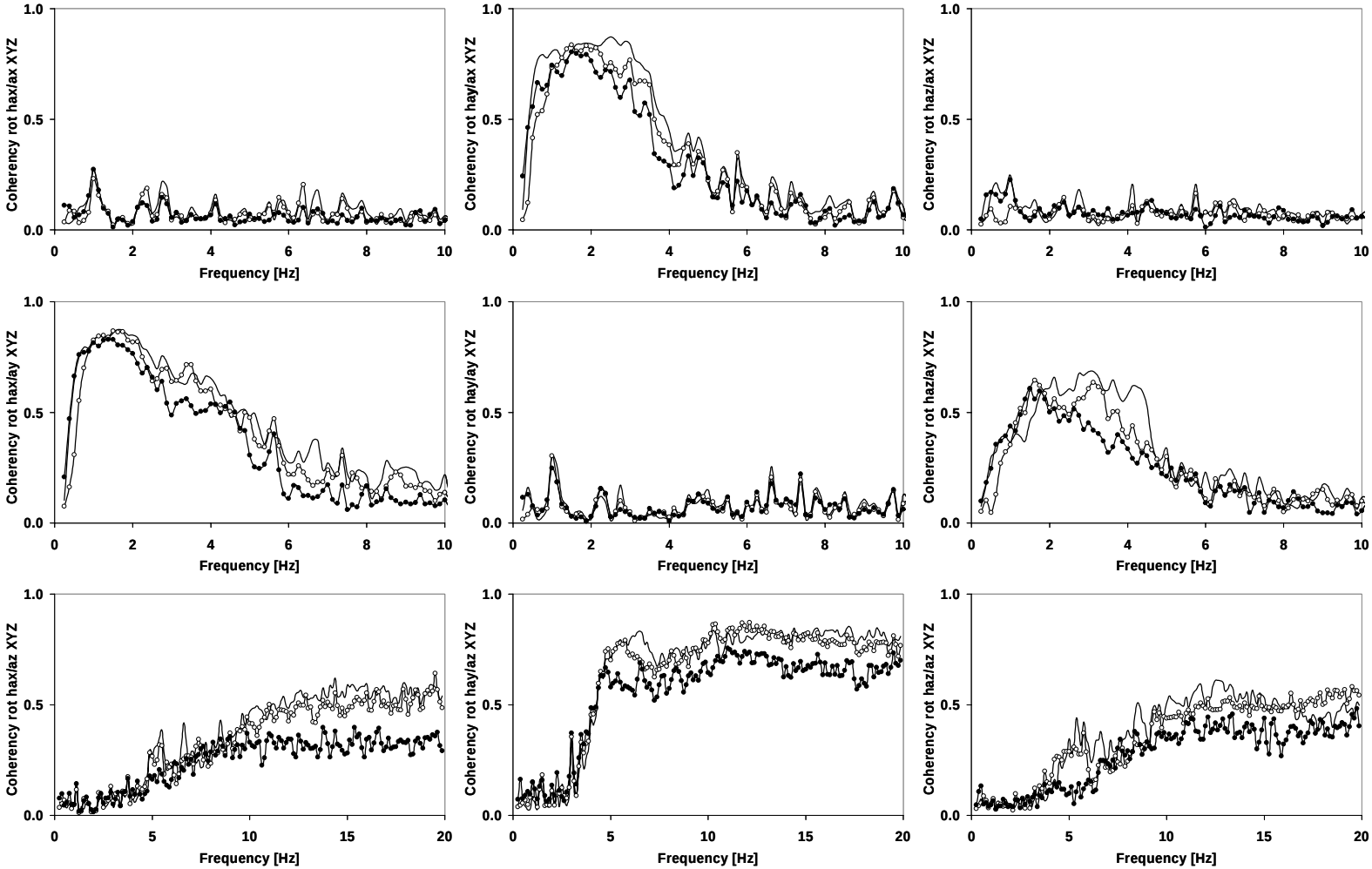

Figure 18. Mean values (MV) of the coherencies associated with the seat-to-head transfer functions during three-axis vibration simultaneously in X-, Y-, and in Z-axis. The translational seat accelerations were related to the rotational head accelerations around x-direction (left), around y-direction (middle) and around z-direction (right). I1 (▬▬), I2 (○), I3 (●).a - acceleration at the seat. ha - acceleration of the head, rot hx - roll acceleration at the head, rot hy - pitch acceleration at the head, rot hz - yaw acceleration at the head.

2 Development and validation of a practical model for the prediction of spinal stress caused by WBV

The subcontractor "Wölfel Beratende Ingenieure" extended the existing linear FE-model developed within the research project 5162 of the German Federal Institute for Occupational Safety and Health (FIOSH) (Hofmann et al. 2003**)** and adapted it to different postures, verified the model together with other partners, and – after the necessary modifications - scaled the model with respect to representative anthropometric characteristics of European drivers (Hofmann, 2005, 2006).

2.1 Extension and adaptation of the FE-model to postures of European drivers

In order to compute the model outputs for the combined vibration excitations measured by partners at the contact points buttocks, back, hands and feet, the existing models and Matlab-files had to be extended. In the FE-model additional calculation steps for the horizontal (X, Y) excitations with adapted boundaries for the four contact points have been added. The Matlab-files used for model generation have been adapted to handle these model modifications.
First the existing model has been adapted to the typical postures of drivers of different machines chosen by WP5 partners UMUH and UTRS Trieste. These postures are defined by model angles according to Figure 19 with resulting disc angles shown in Table 2 with positive angles designating an downward inclination of the anterior part of the disc. Model size is that of the 50^{th} male percentile (mass: 74.4 kg, body height: 1.745 m, Hofmann et al. 2003). The angles have been identified by measuring them on photographs of 17 different workers in their typical working posture on their different machines. Afterwards similar postures have been grouped and the measured angles have been averaged. The corresponding model angles are shown in Figure 19 and Table 3.
A comparison between the models is given in Figure 20 and all the comparisons between models and drivers are shown in Figure 21 - Figure 25.

Table 2 Inclination angles of the disc

	T12/L1	L1/L2	L2/L3	L3/L4	L4/L5	L5/S1
forwarder	-19.16	-20.72	-19.78	-14.67	-4.56	8.65
harvester	-15.94	-18.14	-17.82	-13.31	-3.81	8.88
group1	-16.43	-18.54	-18.12	-13.53	-3.93	8.85
group2	-19.31	-20.84	-19.87	-14.73	-4.60	8.64
group3	-9.57	-12.77	-13.68	-10.49	-2.31	9.31

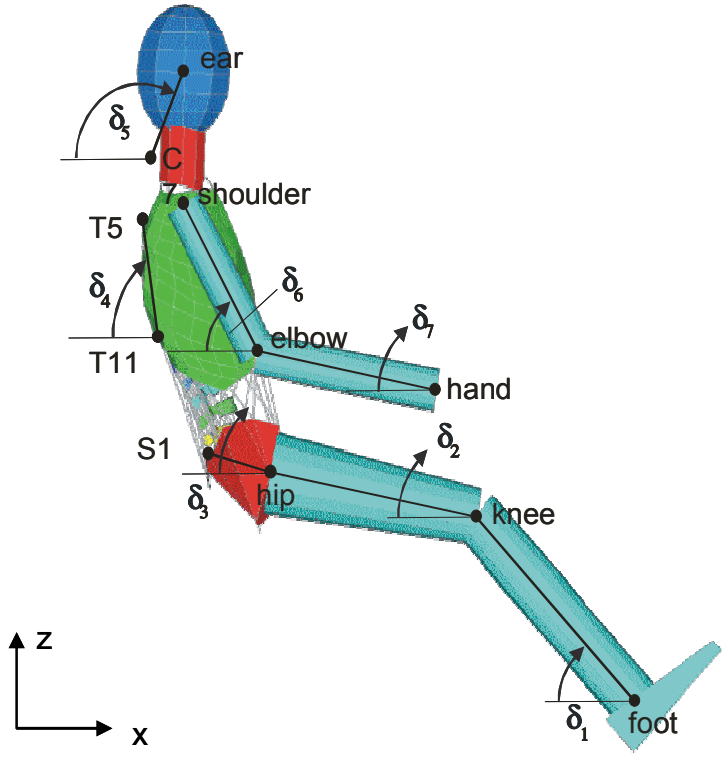

Figure 19. Model angles

Table 3. Model angles [deg] according to Figure 19

Model	Machines	δ1	δ2	δ3	δ4	δ5	δ6	δ7
1	Group 1 (c_1,p_1,p_3,p_4)	72	7.33	18	92.67	129.33	48.67	-6
2	Group 2 (c_4,c_5,p_2)	68	11.75	18	89.5	119.5	43.67	25.5
3	Group 3 (c_3,c_6)	64	2	18	100	125.5	75.42	6.08
4	harvester	75.5	8	18	89.67	121.67	75.75	9.25
5	forwarder	84.7	7.9	18	93.2	122	76.9	13
6	Upright, hands in the lap, no back support, cf. Figure 26	90	0	24.8	90.6	109.9	-	-

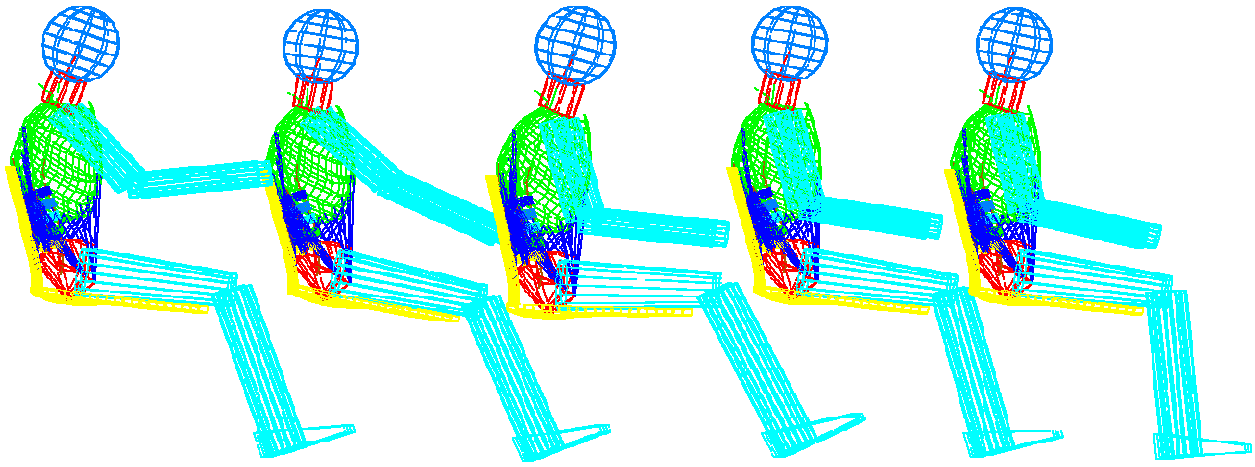

Model 1 (c_1,p_1,p_3,p_4) **Model 3 (c_3,c_6)** **Model 5 (harvester)**

Model 2 (c_4,c_5,p_2) **Model 4 (forwarder)**

Figure 20. Comparison of the models

Figure 21. Model 1, Machine Group 1 (c_1,p_1,p_3,p_4)

Figure 22. Model 2, Machine Group 2 (c_4,c_5,p_2)

Figure 23. Model 3 Machine Group 3 (c_3,c_6)

Figure 24. Model 4 (Forwarder)

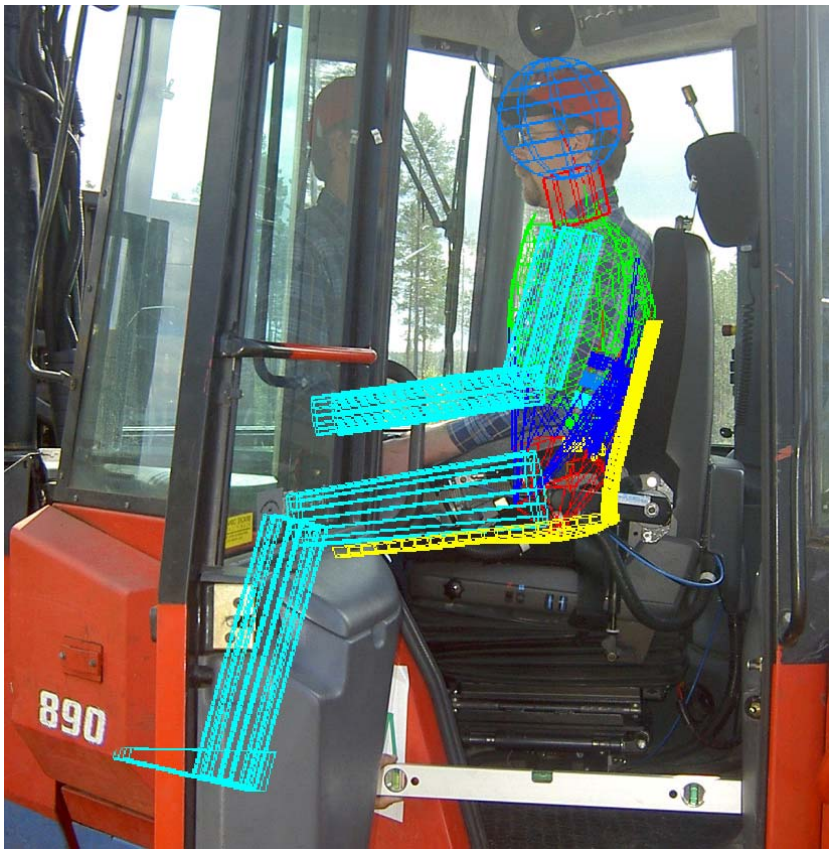

Figure 25. Model 5 (Harvester)

2.2 Validation of the FE-model

For the models defined in section 2.1, the FE-calculations have been performed to determine the mechanical impedance, the apparent mass and the transfer functions to the head. According to the requirements of UsS and UMUH an additional posture of the model (model 6, see Figure 26) has been generated. This posture is described as sitting upright with hands in the lap and without back support (Hofmann, 2005). The model angles δ_6 and δ_7 are no longer used, they automatically result from the position of the hands on the thigh. Data for validation of this posture were provided by the partner UoS.

Validation of the model according to the data provided by FIOSH. The apparent mass data from FIOSH for z-excitation shows a quite high peak at resonance. This peak is significantly higher than that of the simulated data. For the x-excitation the simulation data corresponds much better (see Figure 27 and Figure 28).

Validation of the model according to the data provided by UoS. The only data provided is the apparent mass for z- and x-direction. No transmissibility data was available. The comparison of the model data with that from UoS shows quite good correlation of the model data to the

measurement data, but again the maximum at resonance for z-excitation of the calculated apparent mass is significantly higher (see Figure 27 and Figure 28). Due to the lack of measurement data for y-axis a comparison could not be done.

Due to the quite good compliance of the two measurements and the significant difference to the simulation data for z-excitation an adaptation of the model was necessary. The higher resonance values of the measurements indicated that the initial damping of the model was too high. Therefore, an adaptation of the damping in z-direction was performed. The results are shown in Figure 27 as well. For the modulus a very good correlation could be achieved, the phase has a constant offset, but the characteristic matches very well.

For the x-excitation the simulation results correspond very well to the measured data and therefore no model adaptation was performed.

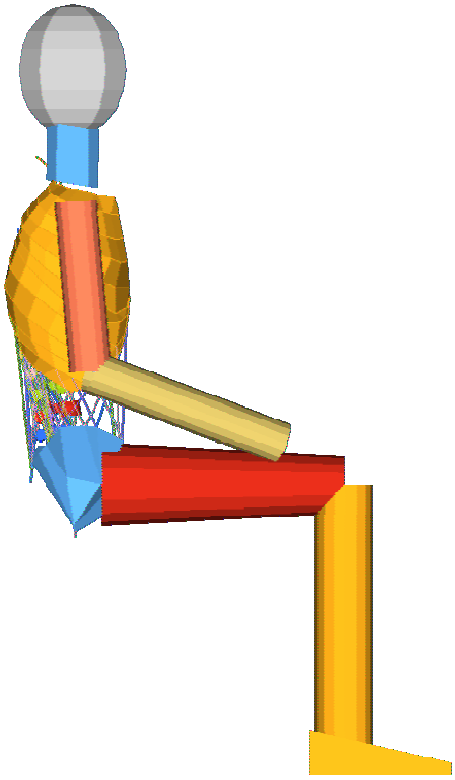

Figure 26. Posture of model 6, hands in the lap, angles cf.

.

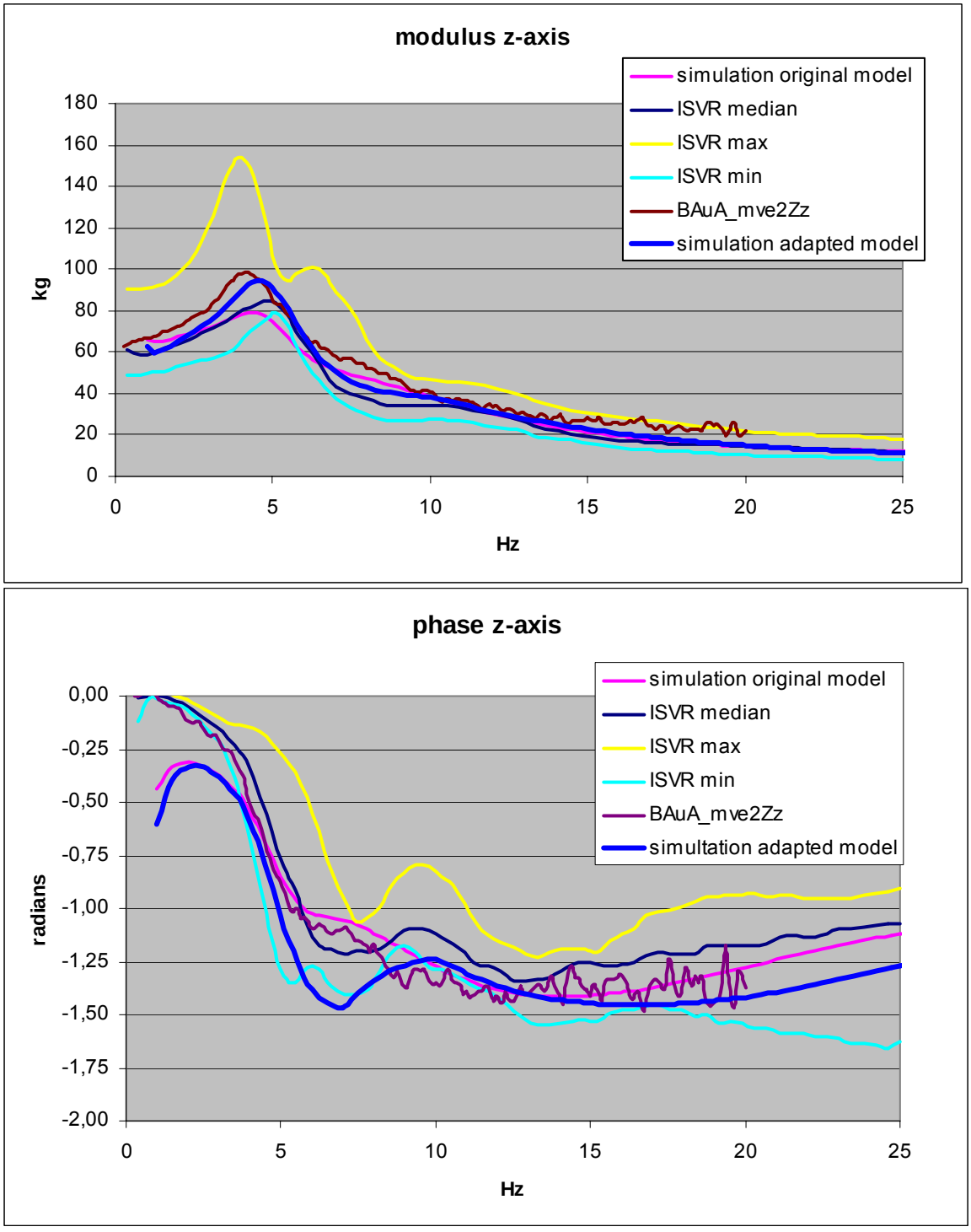

Figure 27. Comparison of model data with measurement data, apparent mass for z-direction

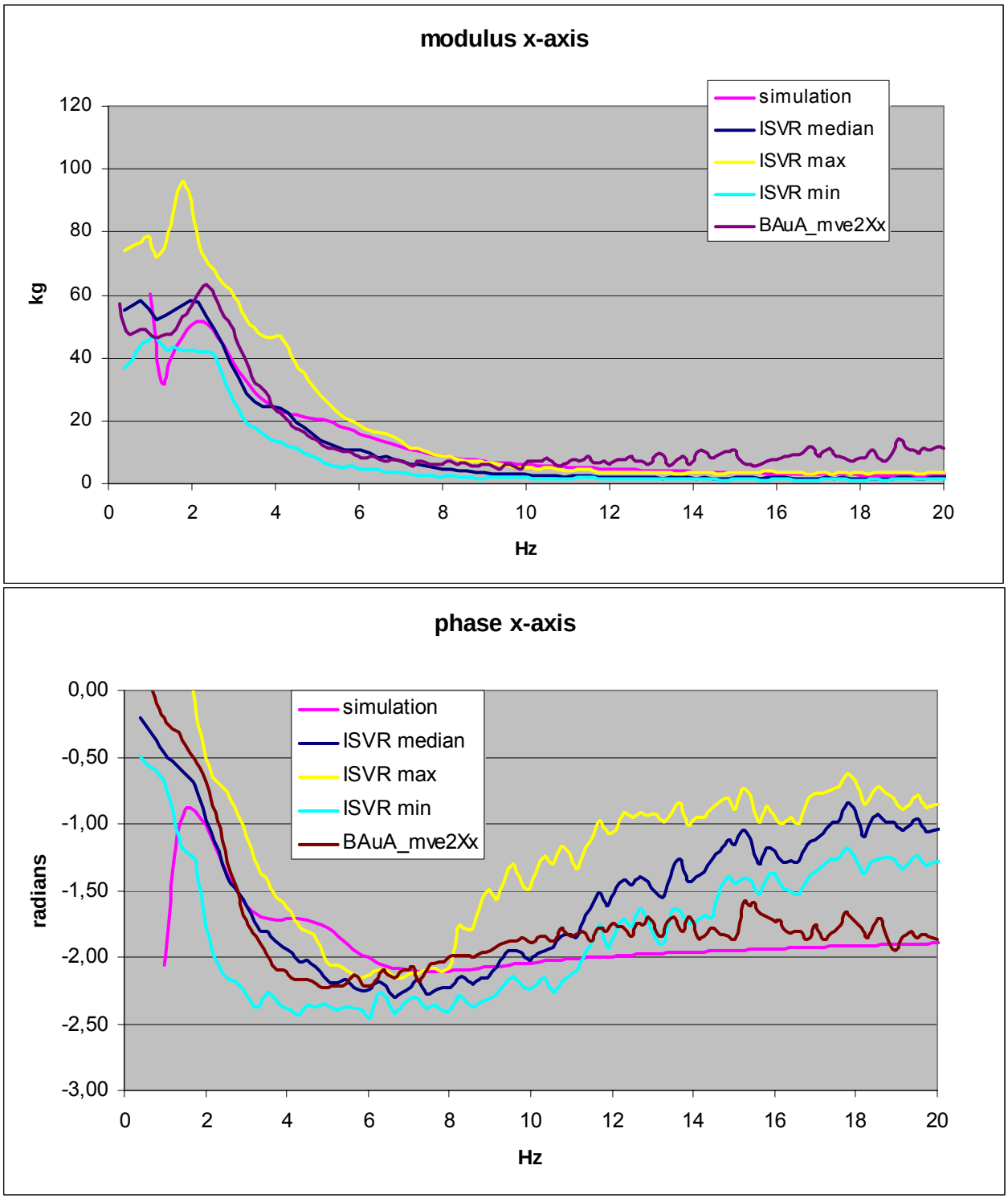

Figure 28. Comparison of model data with measurement data, apparent mass for x-direction

2.3 Scaling of models with respect to representative personal characteristics of European drivers

2.3.1 Anthropometric basis for the scaling of the models.

The aim was to set up a maximum of 10 classes of combinations of personal characteristics that reflect the normal variability of stature of European drivers and permit a sufficient assignment of single cases. Partners of Work Package 5 collected values of the age, body mass and body height for drivers of heavy machines. The data were registered by WP5 partners Trieste, UMUH, and AMC using questionnaires in Italy, Sweden and the Netherlands for drivers of harvesters, forwarders, wheel loaders, fork lifts, and excavators (N=1163 drivers). The machines were selected based on the possible health risks for the lumbar spine caused by whole body vibration.

The scaling of the models should allow the user to select a suited model for an individual driver or for a representative fraction of drivers in order to calculate the internal stress and as prerequisite for the prediction of the health risk related to a certain WBV-exposure.

The statistical analyses of personal characteristics were performed with SPSS-PC.

The body mass index (BMI = body mass / body height^2 [g/cm^2]) was calculated as an additional parameter to characterize the stature of drivers. Table 4 illustrates mean values and characteristic quantities which describe the population of European drivers. Figure 29 illustrates the distribution of age, Figure 30 the distribution of body mass, body height and BMI. The body mass and the body height were weakly correlated in the whole sample (cf. Figure 31). If the model would be scaled primarily according to several classes for body height (with the related mean body mass) and/or several classes for body mass (with the linked mean body mass), the resulting combinations of body mass and body height would not be well suited to reflect the stature of European drivers. Considering the former experience with model calculations for "model families" (Seidel et al. 2001), the body mass index (BMI) was considered.

Table 4. Personal characteristics of European drivers

		Age [year]	Body mass [kg]	Body height [cm]	BMI [g/cm*cm]
N	Valid	1153	1163	1163	1163
	Missing	10	0	0	0
Mean		42.9848	84.5993	178.2919	2.65942
Median		43.0000	83.0000	178.0000	2.61224
Std. Deviation		9.97484	13.14186	7.25395	.365792
Minimum		18.55	50.00	155.00	1.759
Maximum		67.00	165.00	201.00	5.327
Percentiles	5	26.2170	66.0000	168.0000	2.16049
	25	35.8700	75.0000	173.0000	2.42215
	50	43.0000	83.0000	178.0000	2.61224
	75	50.0000	92.0000	183.0000	2.84055
	95	59.0000	108.0000	190.0000	3.32150

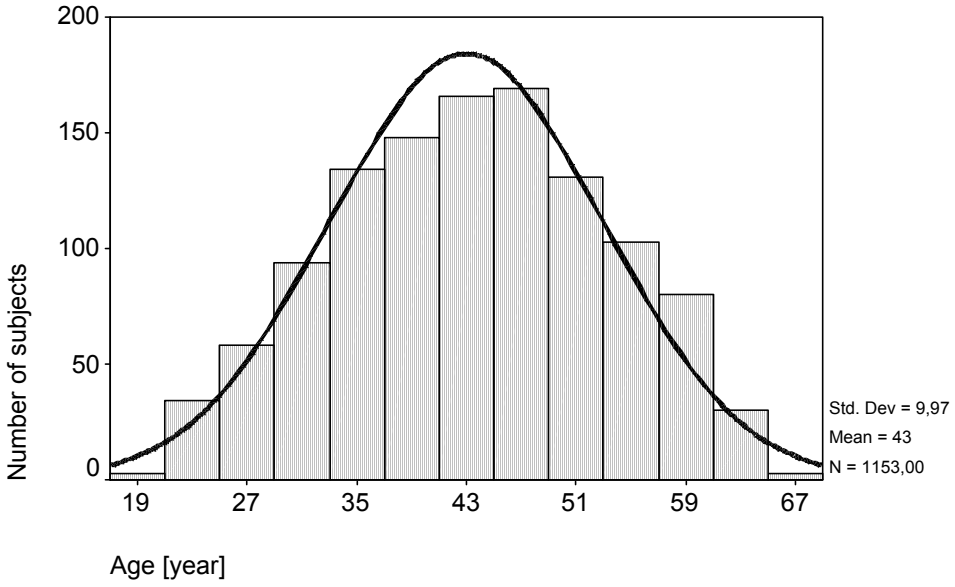

Figure 29. Distribution of the age in the whole sample of 1163 European drivers (age data missing for 10 drivers)

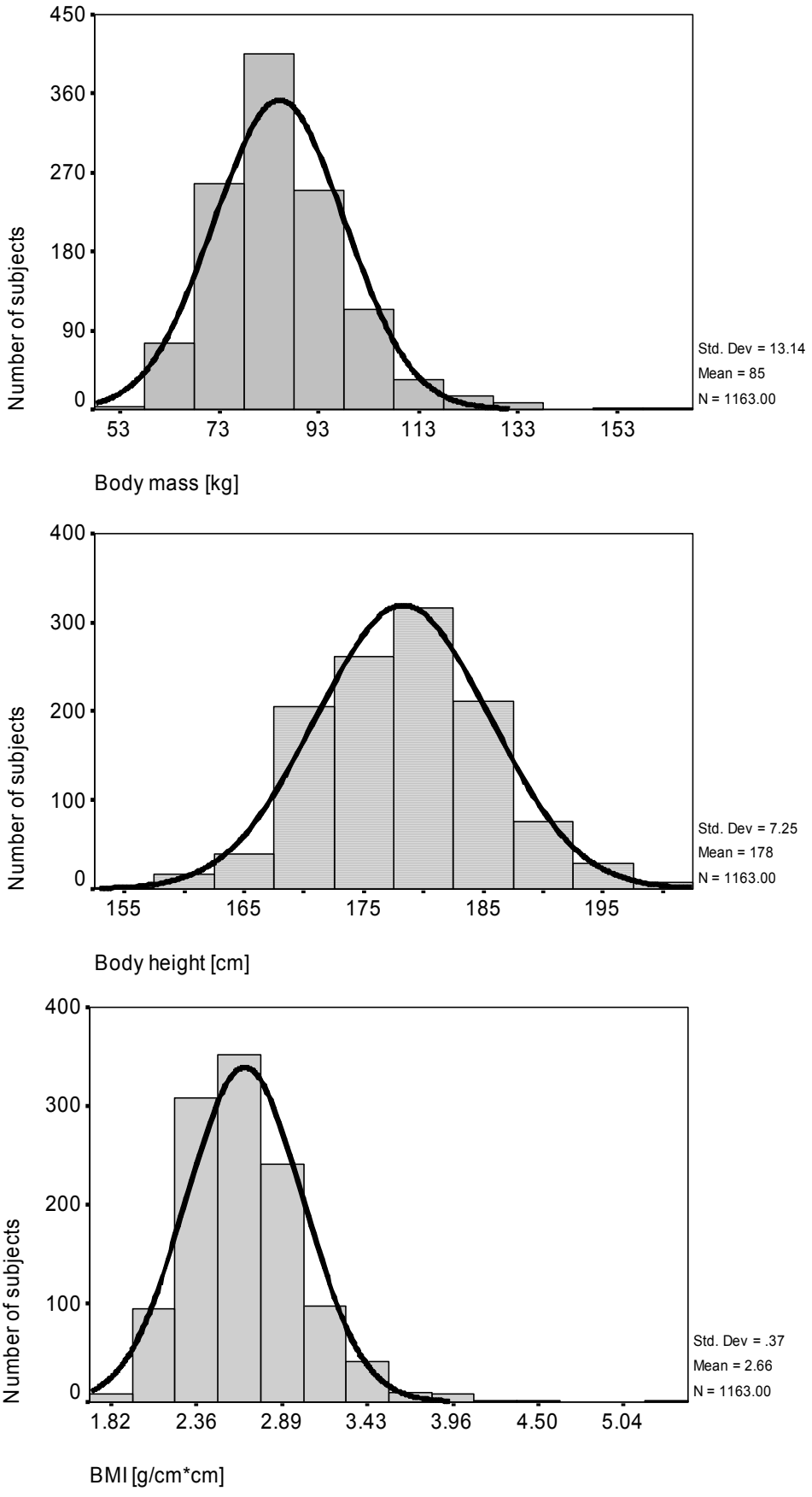

Figure 30. Distribution of the body masses (top), the body heights (middle) and the body mass indices (bottom) of the whole sample of 1163 European drivers

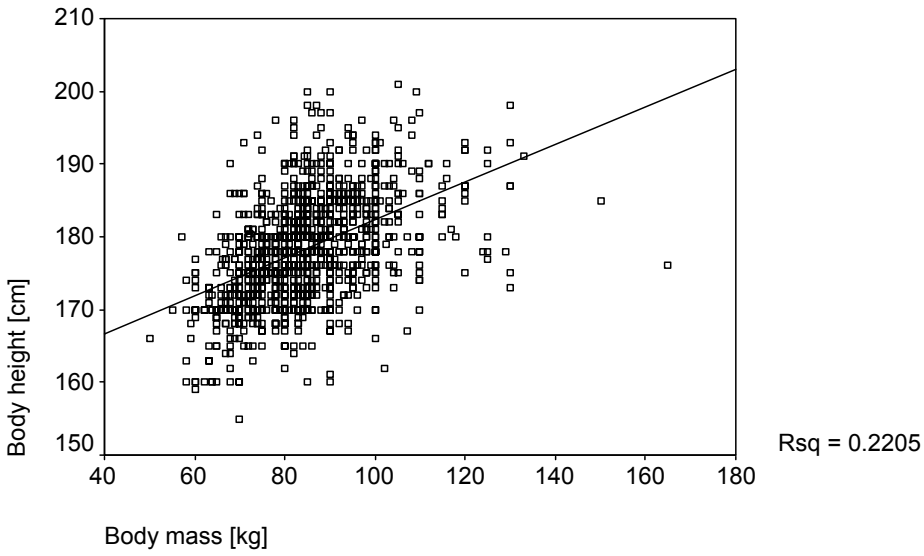

Figure 31. Scatterplot of the relation between body mass and body height. Rsq – explained variance.

The BMI as the relation between body mass and the squared body height was a parameter which takes into account both available parameters as a measure to describe the stature of a subject. A low BMI indicates a slim stature, a high BMI a more stocky stature. Figure 32 illustrates the good correlation between body mass and BMI, and the missing correlation between body height and BMI (Hinz and Seidel, 2006).

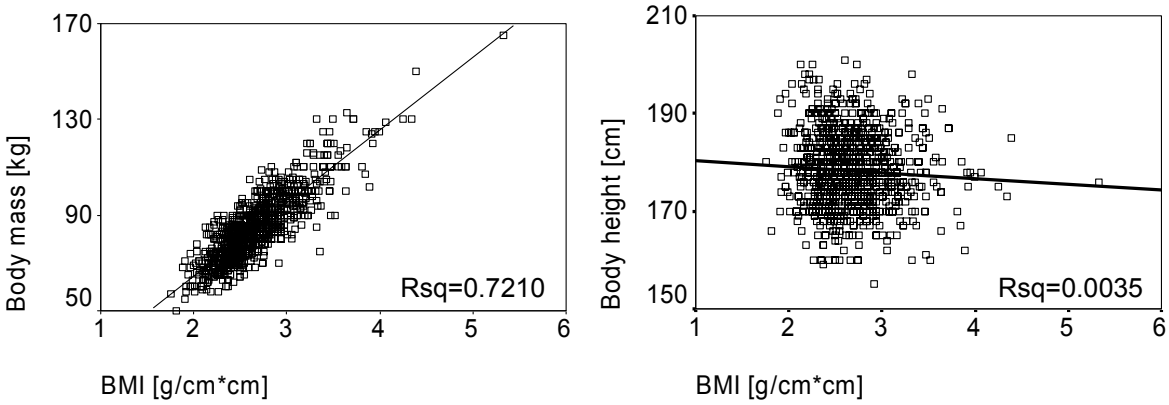

Figure 32. Scatter plots of the relations between body mass and BMI (left), and between body height and BMI (right). Rsq – explained variance.

The median of the BMI of the whole sample was 2.61224 [g/cm^2]. The sample was divided into two main groups: BMI ≤ 2.61 g/cm^2 (N=575, BMI1) and BMI > 2.61 g/cm^2 (N=588, BMI2). In order to allow a better suited assignment of single cases to a class characterised by a combination of body mass and body height, ranges of percentile groups for the body mass were determined (Figure 33) for two subgroups below or equal (BMI1) and above (BMI2) the median of the BMI (Table 5 and Table 6, Figure 34 and Figure 35).

The variances explained by linear regressions were clearly higher for the two subgroups (Figure 34 and Figure 35) than for the whole sample (Figure 31).

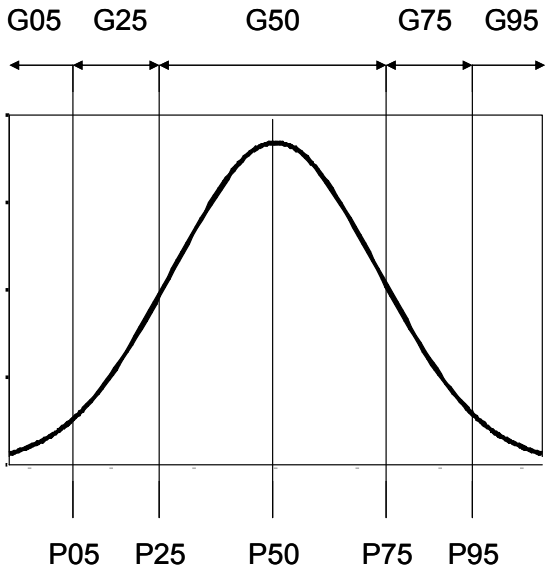

Figure 33. Schematic diagram to illustrate the borders of the selected groups

Table 5. Descriptive statistics of the group BMI ≤ 2.61224 [g/cm^2]

		BMI [g/cm^2]	Body mass [kg]	Body height [cm]	Age [year]
N	Valid	575	575	575	568
	Missing	0	0	0	7
Mean		2.38255	76.1254	178.6113	41.1586
Median		2.42123	75.0000	178.0000	41.0000
Std. Deviation		.159117	8.02086	7.50800	10.20924
Minimum		1.759	50.00	159.00	18.55
Maximum		2.609	105.00	201.00	67.00
Percentiles	05	2.07612	63.0000	168.0000	24.6095
	25	2.28571	70.0000	173.0000	33.1425
	50	2.42123	75.0000	178.0000	41.0000
	75	2.50135	82.0000	183.0000	48.4550
	95	2.58853	90.0000	192.0000	59.0000

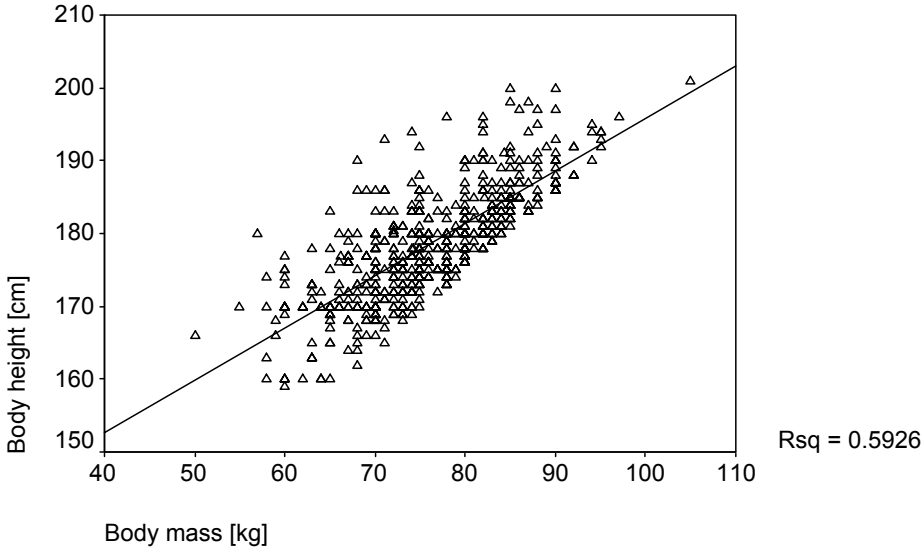

Figure 34. Scatterplot of the relation between body mass and body height for the group with BMI ≤ 2.61 [g/cm^2]. Rsq – explained variance.

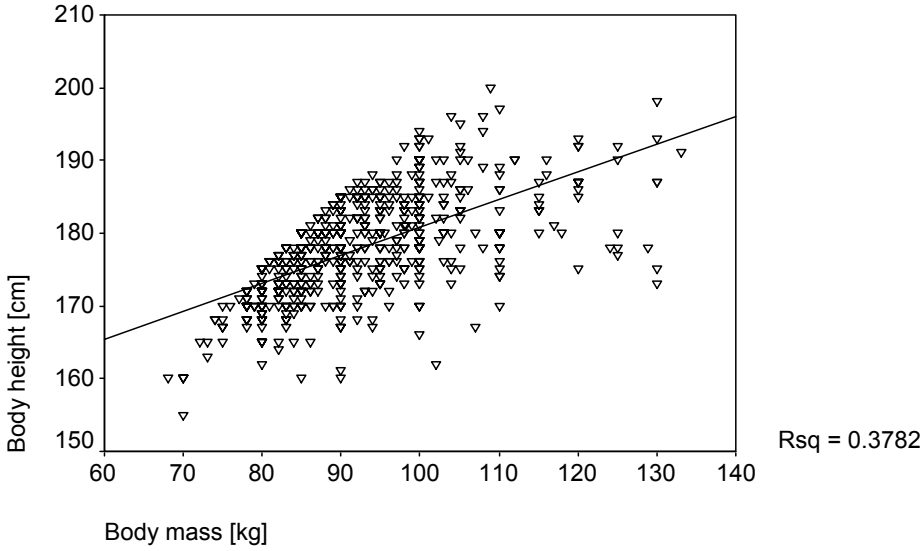

Figure 35. Scatterplot of the relation between body mass and body height for the group with BMI > 2.61 [g/cm^2]. Rsq – explained variance.

Table 6. Descriptive statistics of the group BMI > 2.61224 [g/cm2]

		BMI [g/cm^2]	Body mass [kg]	Body height [cm]	Age [year]
N	Valid	588	588	588	585
	Missing	0	0	0	3
Mean		2.93017	92.8859	177.9796	44.7580
Median		2.84055	90.0000	178.0000	45.0000
Std. Deviation		.302647	11.82595	6.98889	9.41707
Minimum		2.612	68.00	155.00	20.24
Maximum		5.327	165.00	200.00	65.00
Percentiles	5	2.62346	78.0000	167.0000	29.0000
	25	2.71620	85.0000	173.0000	38.0000
	50	2.84055	90.0000	178.0000	45.0000
	75	3.05921	100.0000	183.0000	52.0000
	95	3.47195	115.5500	190.0000	59.4540

Table 7 and Table 8 provide the results of the groups selected for the scaling of models.

Together with the consideration of a typical posture the percentiles of each BMI-group can help to select the suited model to estimate the effects of vibration on the health for a practical case.

Table 7. Ranges of age, body mass (BM), body height and body mass index (BMI) for five percentile groups (P) of body mass for 5, 25, 50 75 and 95 percentile of European drivers with a BMI ≤ 2.61224 [g/cm^2]

	N	Minimum	Maximum	Mean	Std. Deviation
P05=63kg BM < 63 kg					
Age [year]	26	19.00	65.00	44.3542	11.44982
Body mass [kg]	26	50.00	62.00	59.1538	2.41151
Body height [cm]	26	159.00	180.00	168.8077	5.69223
BMI [g/cm*cm]	26	1.759	2.422	2.08286	.168339
P25=70 kg 63 kg ≤ BM < 70 kg					
Age [year]	81	21.00	63.69	39.5377	10.72616
Body mass [kg]	82	63.00	69.00	66.4537	1.93781
Body height [cm]	82	160.00	190.00	171.6098	5.79646
BMI [g/cm*cm]	82	1.884	2.591	2.26301	.149643
P50=75 kg 70 kg ≤ BM < 82 kg					
Age [year]	332	18.55	67.00	41.2302	9.85251
Body mass [kg]	336	70.00	82.00	75.6768	3.82060
Body height [cm]	336	165.00	196.00	177.8586	5.50537
BMI [g/cm*cm]	336	1.906	2.609	2.39526	.132264
P75=82 kg 82 kg ≤ BM < 90 kg					
Age [year]	116	21.00	61.04	41.7831	10.59183
Body mass [kg]	118	82.10	90.00	85.8093	2.32871
Body height [cm]	118	179.00	200.00	186.1949	4.47454
BMI [g/cm*cm]	118	2.125	2.601	2.47768	.099342
P95=90 kg 90 kg ≤ BM					
Age [year]	13	27.95	56.18	37.4654	8.56958
Body mass [kg]	13	92.00	105.00	94.7692	3.44369
Body height [cm]	13	188.00	201.00	193.0000	3.43996
BMI [g/cm*cm]	13	2.472	2.604	2.54389	.048170

Table 8. Ranges of age, body mass, body height and body mass index (BMI) for five percentile groups (P) of body mass for 5, 25, 50 75 and 95 percent of European drivers with a BMI > 2.61224 [g/cm^2]

	N	Minimum	Maximum	Mean	Std. Deviation
P05=78 kg BM < 78 kg					
Age [year]	16	25.00	64.00	46.0406	11.19523
Body mass [kg]	16	68.00	77.00	73.2500	2.56905
Body height [cm]	16	155.00	171.00	165.1250	4.47027
BMI [g/cm*cm]	16	2.622	3.356	2.73537	.181307
P25=85 kg 78 kg ≤ BM < 85 kg					
Age [year]	121	21.00	63.00	44.8479	8.95718
Body mass [kg]	121	78.00	84.00	81.0331	1.91891
Body height [cm]	121	162.00	178.00	171.8017	3.36556
BMI [g/cm*cm]	121	2.612	3.085	2.74785	.110319
P50=90 kg 85 kg ≤ BM < 100 kg					
Age [year]	350	21.36	65.00	44.8946	9.58367
Body mass [kg]	351	85.00	100.00	92.2895	4.92923
Body height [cm]	351	160.00	194.00	179.0171	5.62238
BMI [g/cm*cm]	351	2.623	3.629	2.88497	.192048
P75=100 kg 100 kg ≤ BM < 115 kg					
Age [year]	70	20.24	63.00	44.6257	8.96783
Body mass [kg]	71	101.00	115.00	106.9493	3.88767
Body height [cm]	71	162.00	200.00	183.4648	7.10901
BMI [g/cm*cm]	71	2.707	3.887	3.19178	.276743
P95=115.5 kg ≤115 kg ≤ BM					
Age [year]	28	21.76	60.00	42.2593	9.56199
Body mass [kg]	29	116.00	165.00	125.9621	10.22666
Body height [cm]	29	173.00	198.00	184.8621	6.71206
BMI [g/cm*cm]	29	3.213	5.327	3.70490	.460250

2.3.2 Results of scaling of the FE-models

The anthropometric data (cf. Table 7 and Table 8) of the body mass and body height in the two BMI-groups do not provide information on the distribution of mass within the human body. With a certain probablity, a higher percentage of body mass was assumed at the waist for the group BMI2 (BMI > 2.61 g/cm^2). A possible influence of the waist-circumference was therefore studied with special models. Depending on the data material available it is sometimes impossible to fully transfer the individual body masses of the model. Then those masses not transferred are scaled by the scaling factor of the body height. In the course of project the data sets of the dirvers were sub-divided following the BMI (Body-Mass-Index) into two groups. This has led to the question whether or not it is reasonable to generally raise the waist circumference for test persons with high BMI or to continue to assume a constant distribution. Different modifications and adaptations of models were tested, including completely customised models, i. e. models reflecting personal characteristics of one individual (Harvester 1), particularly with regard to the waist circumference. The apparent mass and time histories of intervertebral disc forces were calculated with these modifications of FE-models. Summarising the results of these special examinations it was concluded that only slight differences between the modelling variants appear when solely adapting the waist circumference. Only a complete customisation of the model led to a clear distinction. The differences based on a modification of the waist circumference are that slight so that a relatively random increase for the models of group BMI > 2.61 g/cm^2 is not applicable, whereas a complete customisation leads to extreme differences. Therefore, the complete customisation might be a future promising approach for special individual cases.

By applying these scaling factors to the five postures defined in section 2.1, a total of 50 models were generated. These models are simulated by transerf functions with the results serving as input for the software design (cf. section 2.4). The factors posture and stature have a clear influence on the calculated spinal forces and risks (cf. Seidel et al. 2006)

The calculated transfer functions are also stored to file in ASCII-format. Thus, for each model a three-dimensional matrix exists with the transfer functions for the different percentiles, excitation points and excitation directions with 10x4x3 cells. For each cell of the matrix a file is generated. The file name and the file header (see below) each clearly specify which transfer functions are contained, e.g.,

Transfer function
Model: harvester
Percentile: BMI1m05
Excitation: G
Output Format:s
Columns: frequency, x, y, z forces for disk level 1 - 6

The data structure is shown in Figure 36. After the header the matrix of transfer functions is arranged. In the first three columns the frequency is listed, in the following columns the transfer functions in the x-, y-, z- direction for each disc level are arranged. Thus, in columns 4 to 6 the spinal forces in x-, y- and z- direction for disc level 1 are listed, in 7 to 9 the corresponding data for disc level 2 etc. until disc level 6.

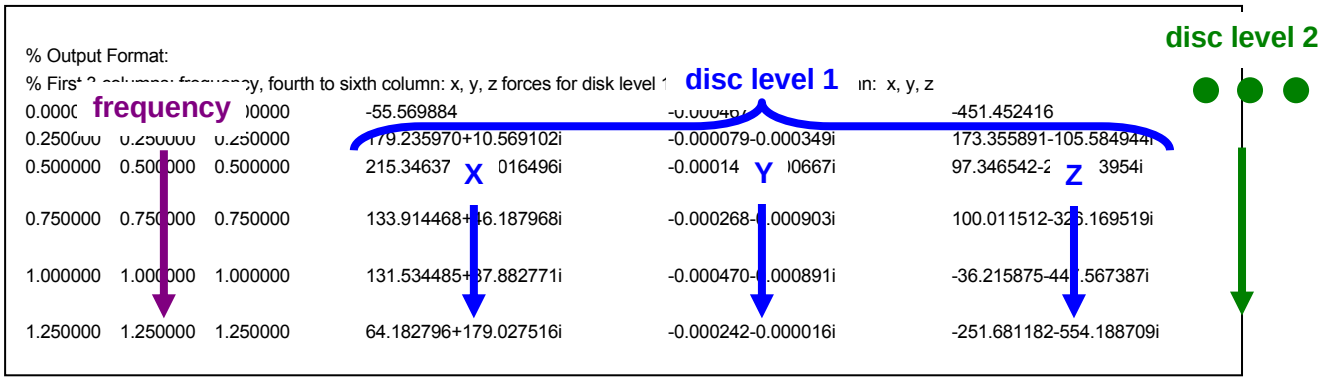

Figure 36. : Data structure of the ASCII-files of the transfer functions

For use within the software described in section 2.4 the results of each model are also stored in a separate MATLAB binary file, named UefuBSK.mat. When using the software, these files must be accessible as described in the installation instructions in section 2.4.

2.4 Software design

This section covers the programming of a software within MATLAB by which - based on input accelerations at the four contact points of the model to the environment (buttock, back, hands, feet) - the resulting forces within the lumbar spine for arbitrary input accelerations can be determined. ASCII-files are used for the data in- and output. The output files contain a header with a clear file description therein.

For an easy handling of the software, a graphical user interface (GUI) has been designed, by which the user can control all necessary inputs (see Figure 37).

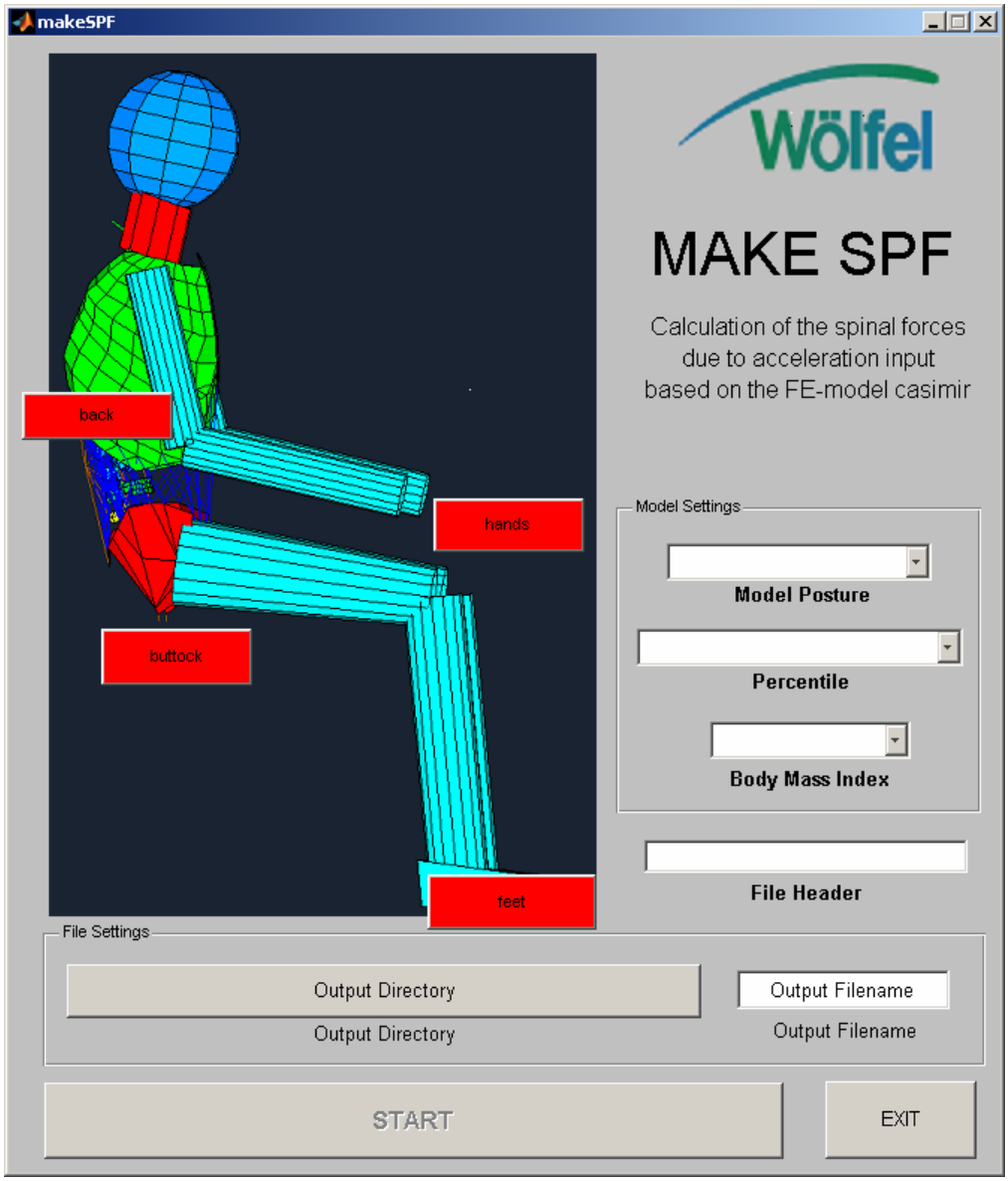

Figure 37. Graphical user interface

The initially red buttons on the left side (within the figure of the model) are used to choose the corresponding input accelerations. By pushing a button, a file dialogue box for selecting the excitation appears (see Figure 38). When a file is selected, the name of the selected file is shown and the corresponding button turns green. If there is no measured acceleration data for a specific point, the user may choose – in dependence on the real situation - either the same acceleration or an other suited input or - if there is no contact of the operator with the machine at this part of the body - a file with zero acceleration (of the same size and resolution as the other accelerations. The latter is **not** recommended for back acceleration, in this case the buttock acceleration should be used. The sampling rate is free (a minimal rate of 0.01 s is

recommended), the file length of the acceleration input is limited to 140,000 samples, but have to be identical for each contact point.

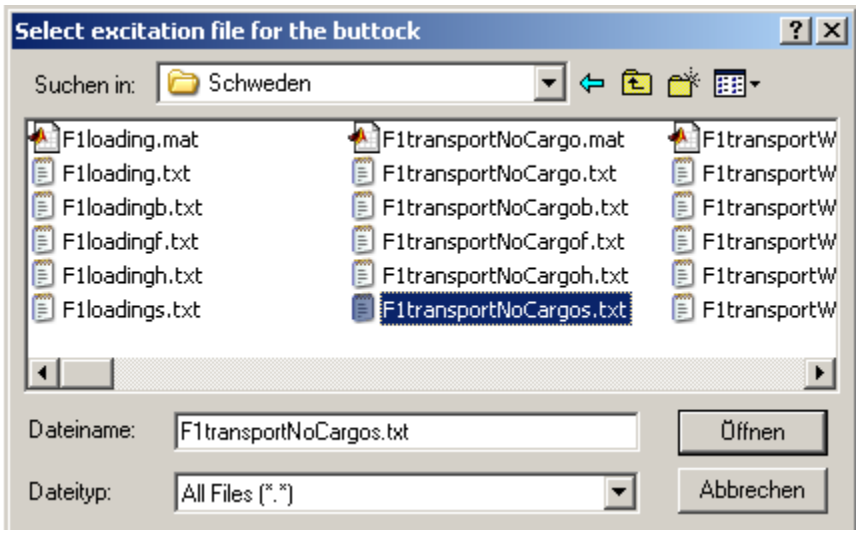

Figure 38. File dialogue box for selecting the excitation

The data has to be formatted within the ASCII-files as follows with signs as indicated in ():

First Column: Time

Second Column: x-acceleration (ventrally – plus)

Third Column: y-acceleration (to left – plus)

Fourth Column: z-acceleration (cranially – plus)

An optional header or footer may be included, but those rows have to start with a “%” to indicate that it is a comment only.

On the right side, the user can specify the model settings he wants to calculate the spinal forces for.

Firstly, the 'Model Posture' has to be defined. Secondly, the 'Percentile' and the 'Body Mass Index' have to be specified (cf. Figure 37).

Afterwards an optional file header (user header) for the output file may be entered. By standard, the following header, specifying the model and the input accelerations, is created:
User header: Test
Model: ….:\.....\forwarder
Percentile: BMI2m95
Seat excitation: …:\.....\forwarder\AnrG_F1_TwoC.dat
Back excitation: …:\.....\AnrL_F1_TwoC.dat

Hand excitation: ….:\.....\AnrH_F1_TwoC.dat
Feet excitation: …:\.....\AnrF_F1_TwoC.dat

Output Format:

First column: time, second to fourth column: x, y, z forces for disk level 1, fifth to seventh column: x, y, z forces for disk level 2, ..

In the file settings box, the output directory shall be defined by pushing the 'Output Directory' button. A special dialogue box opens (see Figure 39) by which the directory can be specified and the file name can be entered directly. Once all the inputs have been performed, the previously deactivated start button is activated. By pushing it, the calculation is started. Depending on length and sampling rate of the input acceleration, this calculation may last shorter or longer, typically less than 3 minutes for an acceleration signal of 60 seconds.

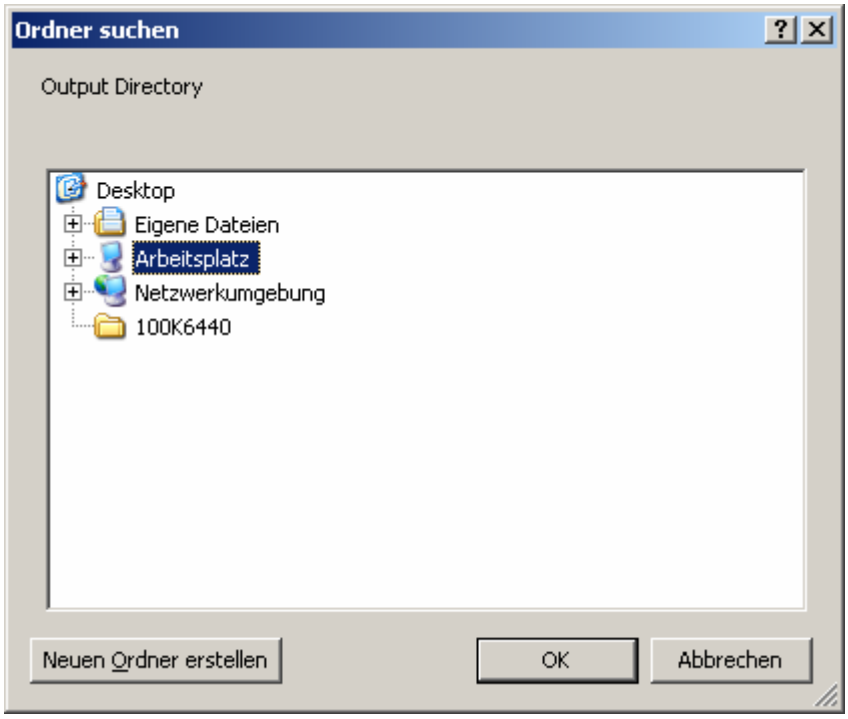

Figure 39. Dialogue for specifying the output directory

The results are stored to file in the frequency- and time-domain with the header described above. To identify the file content for the frequency-domain file, '_freq' and for the time domain file '_time' is added to the file name.

The data structure of the ASCII-files in the time-domain and in the frequency-domain file is identical, except that the real and imaginary parts of the frequency domain files are listed in two separate columns. After the header the result matrix is arranged. In the first column the time or the frequency is listed, in the following columns the spinal forces in the X-, Y-, Z- direction for each disc level are arranged. Thus, in columns 2 to 4 (time domain) and 2 to 7 (frequency

domain) the spinal forces in X-, Y- and Z- direction for disc level 1 are listed, in 5 to 7 and 8 to 13, respectively, the corresponding data for disc level 2 etc. until disc level 6 (see

Figure 40 top and bottom).

The disc levels are ordered from top to bottom, so that level 1 means between vertebra T12 and L1, level 2 between vertebra L1 and L2 etc. until level 6 between vertebra L5 and S1. Due to the structure of the model, the disc at level 1 has a significantly lower stiffness. It does not only represent the stiffness of the disc between T12 and L1, but also partly that of the torso. This leads to an increase especially in the shear force in Y-direction. So the results for level one should be treated with caution.

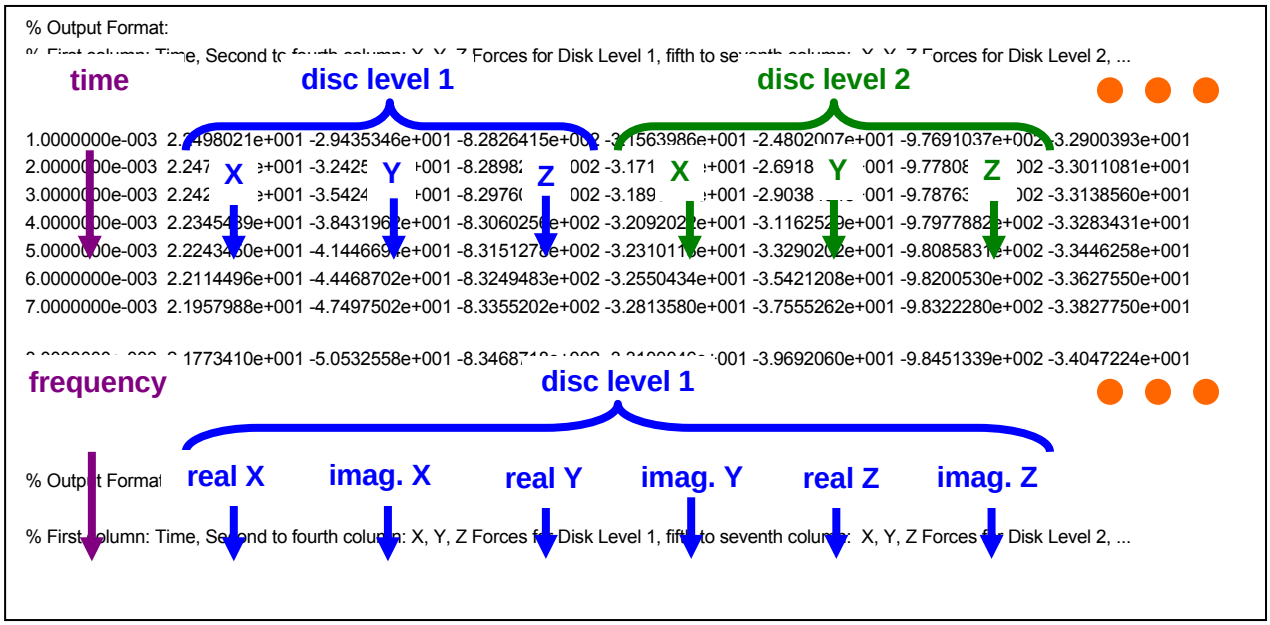

Figure 40. Data structure of the ASCII-files of the disc forces (top: time domain, bottom frequency domain)

The calculated intraspinal forces are also saved as mat-file. This file contains values according to the structure shown in Figure 41 and Table 9. Spectra and time series caused by a single input location for each coordinate-direction can contain portions (due to the modeling) that may cancel each other out by the overlay of the results of different input locations. This is especially the case for the inputs at the backrest and seat surface. Therefore, the user shall use only the results of the combined input. Also for this reason, the user shall never set the inputs of the backrest or seat surface to zero, but always use a real signal or identical signals for both locations. The results of single

inputs require special experience for their interpretation which is only available with the subcontractor WBI.

In the cell-array of the input, the inputs are listed in the sequence 'G', 'F', 'H', 'R'.

In the cell-array of the responses the data structure is as follows:

single forces: Dim1: location of the input ('G', 'F', 'H', 'R')

Dim2: axis of the input x, y, z

Dim3: disc level (1-6, cranial to caudal)

combined forces: 6 intra-spinal forces (1-6, cranial to caudal)

The single cells contain matrices with the corresponding results (x, y, z).

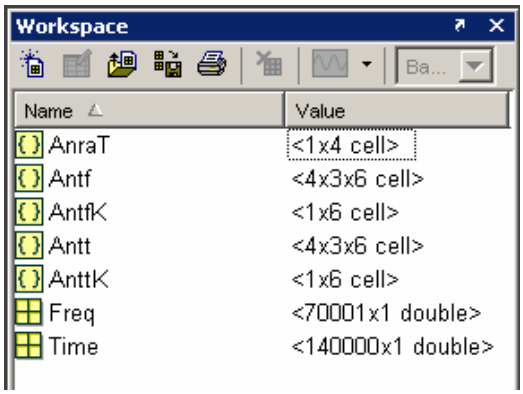

Figure 41 Structure of the Matlab file resulting from model calculations

Table 9. Structure of the Matlab file resulting from model calculations

variable	contents	type
AnraT	time series of the acceleration inputs	1x4 cell-Array
Antf	spectra of the intra-spinal forces caused by single inputs	4x3x6 cell-Array
AntfK	spectra of intra-spinal forces caused by the combined input	1x6 cell-Array
Antt	time series of the intra-spinal forces caused by single inputs	4x3x6 cell-Array
AnttK	time series of intra-spinal forces caused by the combined input	1x6 cell-Array
Freq	frequency vector of the above-mentioned results	1xn double
Time	time vector of the above-mentioned results	1xn double

2.5 Instructions for users

For using this software, MATLAB needs to be installed in revision 7 or higher on your computer and the following MATLAB-files must be accessible. The simplest way to insure this is to copy them in a specially directory, further called installation directory.

makeSPF.m
makeSPF.fig
BSK.m
MYIFFT.m
CasiAntspec.m
MYFFT.m
interpolf.m
AnrImport.m

Additionally the two logos must be in the installation directory: woelfel.png, modell.png.

The results of each model are separately stored in files called UefuBSK.mat and they must be accessible in a subdirectory called <model name> of the installation directory. So the typical path for harvester would be: <installation directory>\harvester\UefuBSK.mat

To start the program from within MATLAB, simply change the current directory to the installation directory and execute makeSPF from the Command Window.

2.6 Results of model calculations - examples

In this chapter some typical results of the testing of the model are shown. The excitation signal is that of forwarder f1 for transport without loading. In Figure 42 this excitation signal for the seat surface is plotted. Figure 43, Figure 44 and Figure 45 show the resulting forces within the intervertebral discs of different levels for the BMI 1 group, 5^{th} percentile.

Figure 46 shows a comparison of different percentiles and Figure 47 shows a comparison of different models.

Additionally different excitation signals with different time length and frequency resolution have been tested.

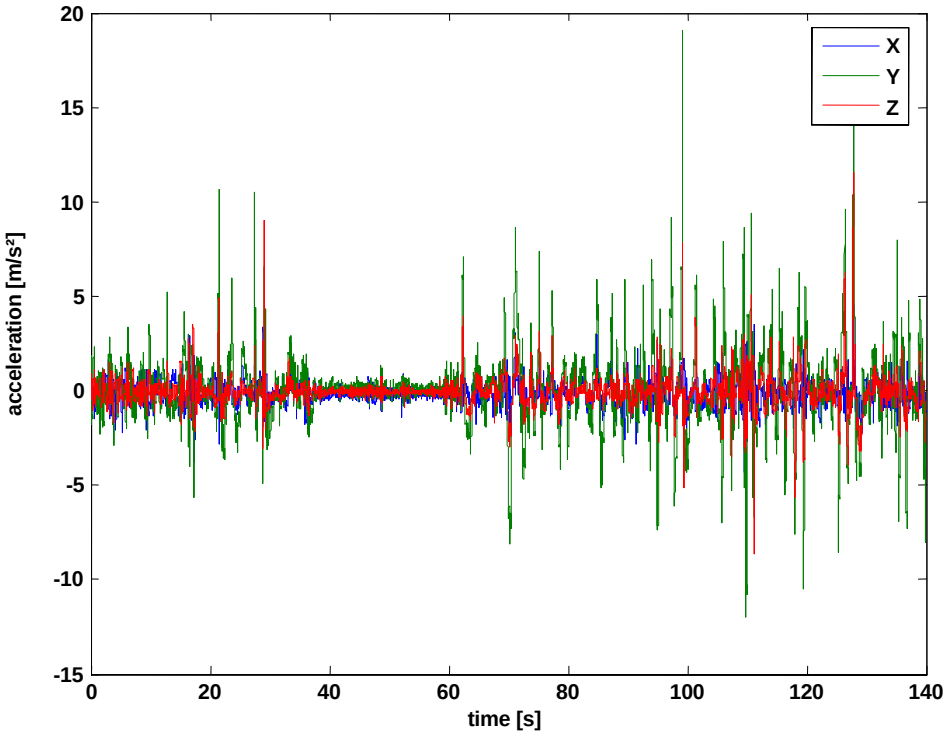

Figure 42. Excitation signals from forwarder f1, transport without load, seat surface

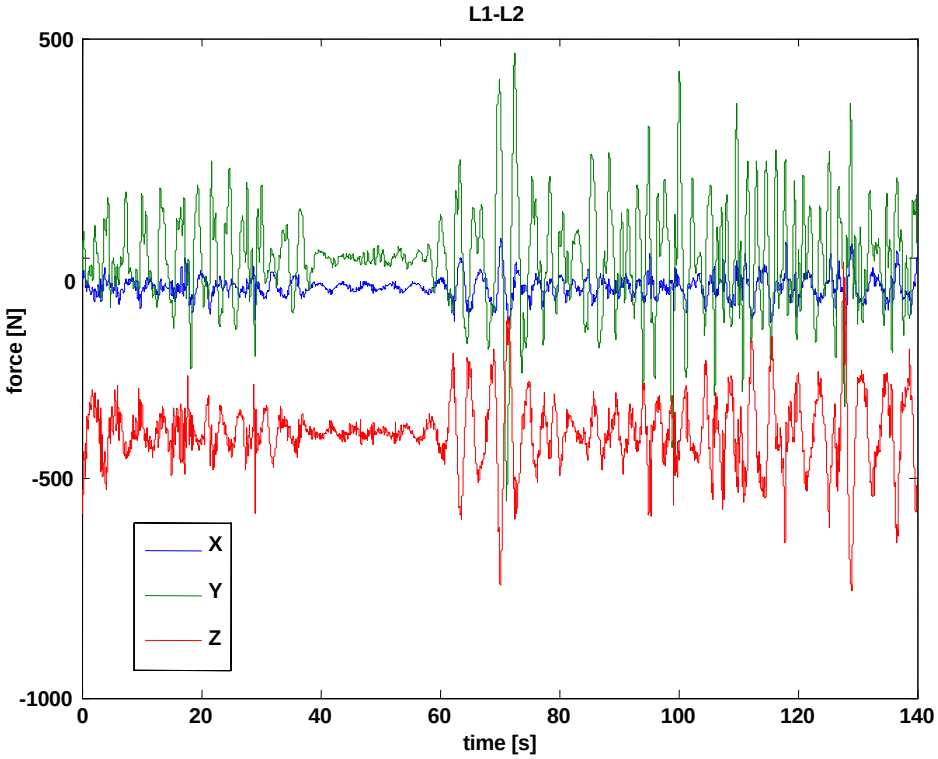

Figure 43. Spinal forces at the level L1/L2 for the 5th percentile BMI1

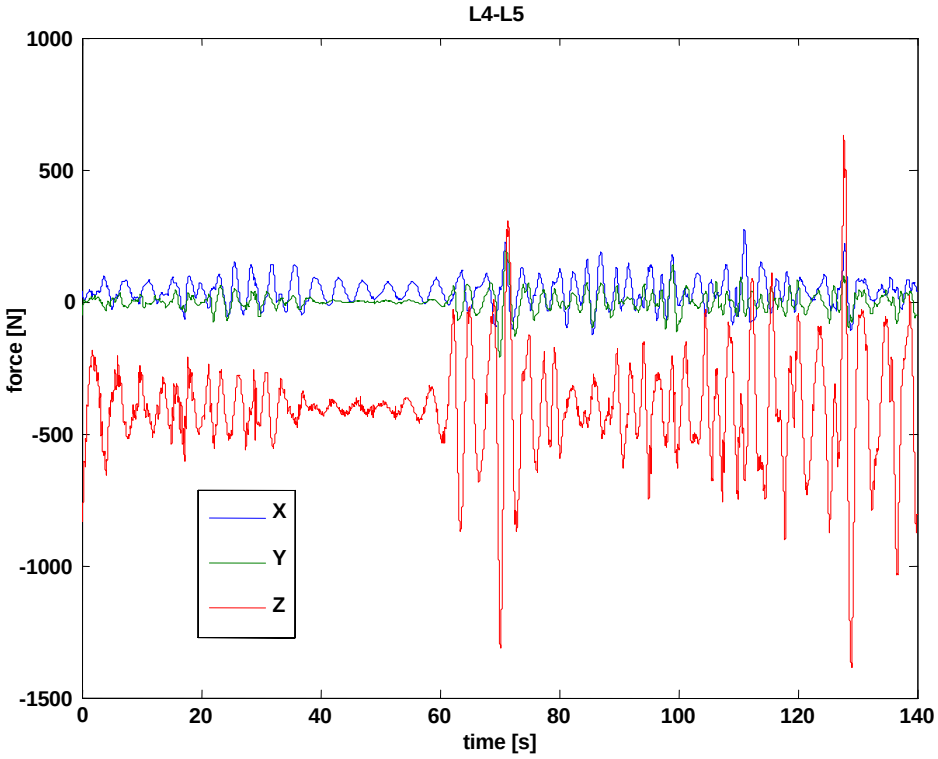

Figure 44. Spinal forces at the level L4/L5 for the 5th percentile BMI1,

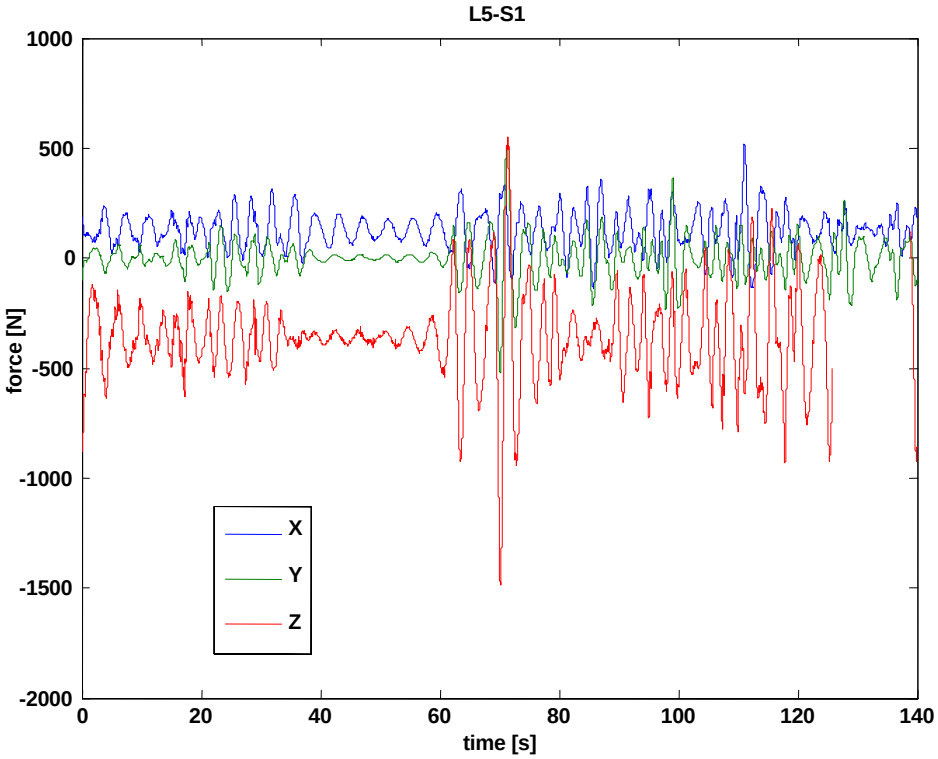

Figure 45. Spinal forces at the level L5/S1 for the 5th percentile BMI1,

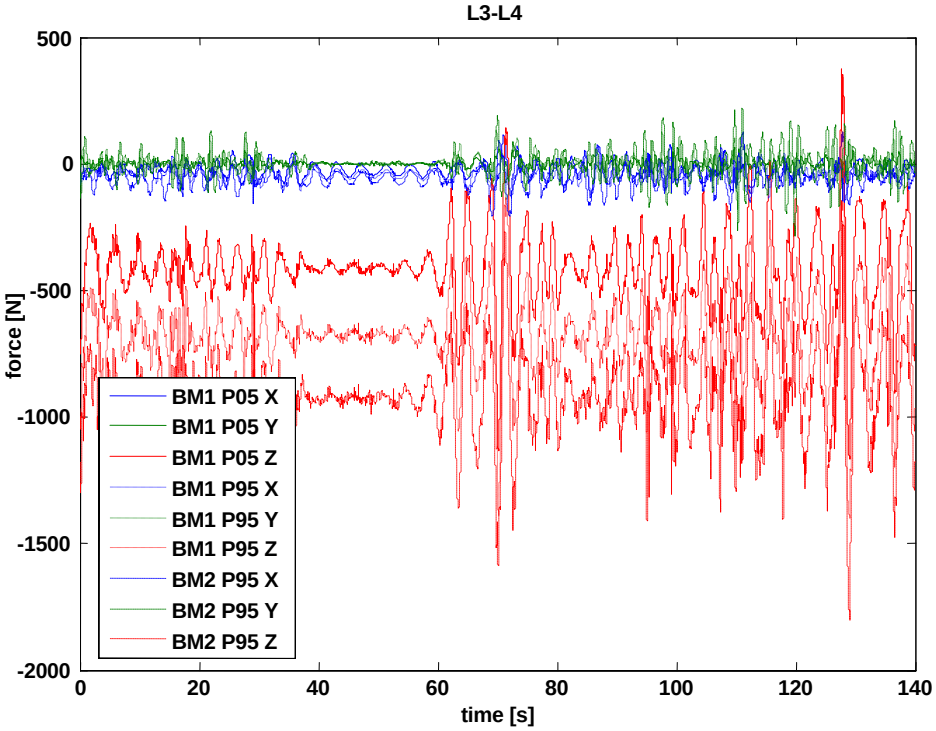

Figure 46. Comparison of the spinal forces in three directions of different statures (percentile and BMI) at the level L3/L4 different percentiles

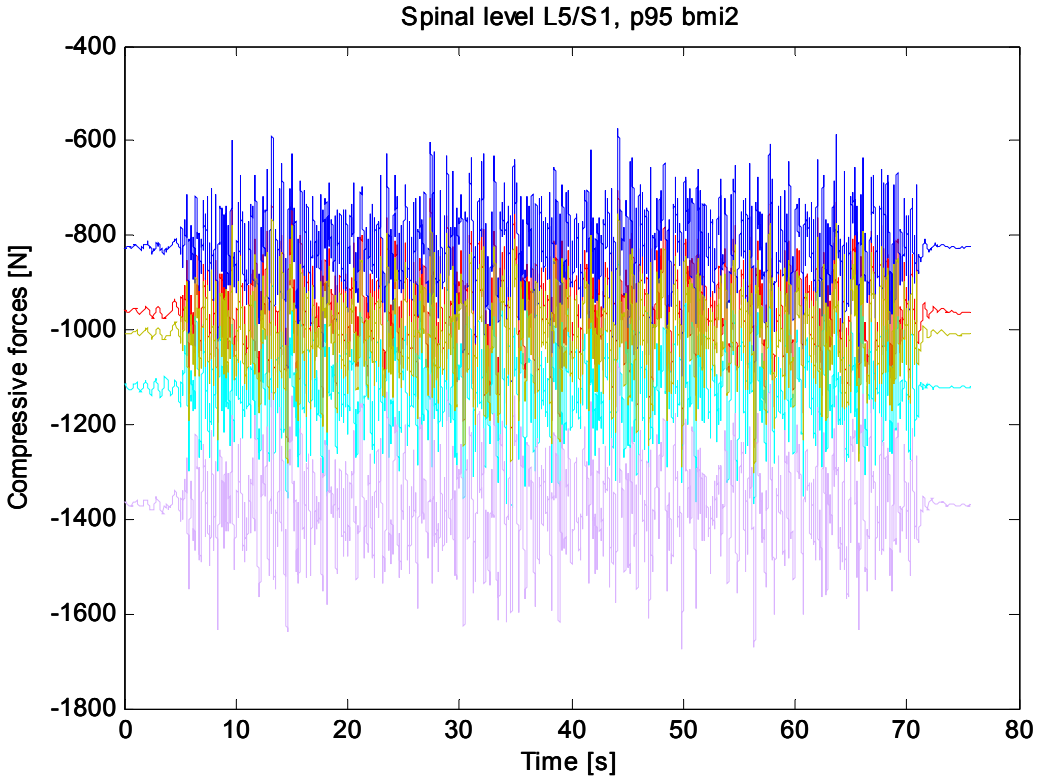

Figure 47. Compressive forces (exposure white noise) calculated for the spinal level L5/S1, the 95th percentile BMI2 with 5 different models/postures: Red – model group3, turquoise – model group 2, purple – model group 3, blue – model forwarder, curry – model harvester

3 References

(1) Hinz B, Menzel G, Blüthner R, Seidel H: Transfer functions as a basis fort he verification of models – variability and restraints. Clinical Biomechanics S1 (2001) S93-S100.

(2) Hinz B, Blüthner R, Menzel G, Rützel S, Seidel H, Wölfel HP: Apparent mass of seated men – Determination with single- and multi-axis excitations at different magnitudes. Journal of Sound and Vibration 298 (2006) 788-809.

(3) Hinz B, Seidel H: Anthropometry of European drivers. Technical Report of the EU-Project VIBRISKS 2006; 23p.

(4) Hofmann J, Pankoke St, Wölfel HP: Individualised FE-model of seated humans and representation of motion segments of the lumbar spine as substructure to determine internal loads during vibration excitation, 188 pp., ISBN 3-86509-030-3, 2003 (in German)

(5) Hofmann J: Verification of the individualised FE-model based on experimental data. Internal Report for EU-Project VIBRISKS 2005.

(6) Hofmann J: Extension, adaptation and scaling of the individualised FE-model to a practical model for the prediction of spinal stress. Internal Report for EU-Project VIBRISKS 2006.

(7) ISO 13090-1. Mechanical vibration and shock – Guidance on safety aspects of tests and experiments with people – Part 1: exposure to whole-body vibration and shock, 1998.

(8) Nawayseh N, Griffin MJ: Non-linear dual-axis axis biodynamic response to vertical whole-body vibration, Journal Sound and Vibration 268 (2003) 503-523

(9) Nawayseh N, Griffin MJ: Non-linear dual-axis axis biodynamic response to fore-and-aft whole-body vibration, Journal Sound and Vibration 282 (2005) 831-862

(10) Paddan GS, Griffin MJ: The transmission of translational seat vibration to the head – 1. Vertical seat vibration. Journal Biomechanics 21(1988a) 191-197

(11) Paddan GS, Griffin MJ: The transmission of translational seat vibration to the head – 2. Horizontal seat vibration. Journal Biomechanics 21(1988b) 199-206

(12) Seidel H, Blüthner R, Hinz B: Application of finite-element models to predict forces acting on the lumbar spine during whole-body vibration. Clinical Biomechanics 16 (2001) Suppl. 1 S57-S63

(13) Seidel H: On the relationship between whole-body vibration exposure and spinal health risk. Industrial Health 43 (2005) , 361-377

4 Appendix A. Index to Figures

5 Appendix B. Index to Tables